

Theory of Transport in Highly Concentrated Electrolytes

Max Schammer,^{1,2} Birger Horstmann,^{1,2,3,*} and Arnulf Latz^{1,2,3,†}

¹German Aerospace Center, Pfaffenwaldring 38-40, 70569 Stuttgart, Germany

²Helmholtz Institute Ulm, Helmholtzstraße 11, 89081 Ulm, Germany

³Universität Ulm, Albert-Einstein-Allee 47, 89081 Ulm, Germany

Ionic liquids are promising candidates for novel electrolytes as they possess large electrochemical and thermodynamic stability and offer a high degree of tunability. As purely-ionic electrolyte without neutral solvent they exhibit characteristic structures near electrified interfaces and in the bulk, both being described theoretically via separate frameworks and methodologies. We present a holistic continuum theory applying to both regions. This transport theory for pure ionic liquids and ionic liquids-mixtures allows the systematic description of the electrolyte evolution. In particular, dynamic bulk-transport effects and interfacial structures can be studied. The theory is thermodynamically consistent and describes multi-component solutions (ionic liquids, highly concentrated electrolytes, water-in-salt electrolytes). Here, we give a detailed derivation of the theory and focus on bulk transport processes of ionic liquids as appearing in electrochemical cells. In addition, we validate our framework for a zinc-ion battery based on a mixture of ionic-liquid and water as electrolyte.

I. INTRODUCTION

The political and social demand for ecologically friendly, low cost, and rechargeable batteries with high energy densities is an increasing research stimulus for the improvement of materials, and the development of novel battery-components.¹ Electrolytes play a key role for the performance of electrochemical systems.² Common types of electrolytes include aqueous electrolytes,³ organic electrolytes,⁴ solid electrolytes,⁵ and recently, ionic liquids (ILs).⁶ ILs have attracted attention in the context of many technologies, including energy management, electrodeposition, bioscience, and biomechanics.⁷ A large number of ILs can be mixed from various cations and anions.⁸ This allows to tailor-cut them into task specific designer electrolytes. Thus, many ILs exhibit a variety of beneficial properties which makes them promising candidates for novel electrolytes.⁹ Their favorable properties include large electrochemical windows, low flammability, or low vapor pressures. Thus, they can be compatible with high voltage electrodes, offer intrinsic safety, or be stable towards air.¹⁰ Furthermore, some ILs suppress dendritic growth during metal deposition.¹¹ Depending on their composition, many ILs are environmentally friendly.¹²

Current theoretical studies concentrate on the bulk,¹³ or on interfacial structures.¹⁴ Unifying approaches describing both scales are rare, but deliver remarkable results.^{15–18} However, a complete unified approach for the dynamic description of ILs, and multi-component IL-mixtures, at bulk and interface, is still missing in the literature. In this article, we present such a unified framework based on the concepts of rational thermodynamics (RT) which we previously applied to electrolytes with neutral solvents.^{19,20} RT provides a thermodynamically consistent framework to model a great variety of non-equilibrium systems. Here, we use RT to derive a continuum transport theory for strongly correlated electrolytes. In this work, we focus on bulk-transport. In a previous

publication,²¹ we showed how to supplement the theory with hardcore interactions and describe the interfacial behavior of ILs. We illustrate our holistic framework in fig. 1.

Molecular/atomistic studies of ILs are based on molecular dynamics (MD) simulations and (classical) density functional theory (DFT) simulations. DFT resolves microscopic ion-properties, delivers detailed insights into the molecular arrangement in the electrochemical double layer (EDL)²² and describes bulk properties like ion-pair formation²³ or small-scale ion-diffusion.²⁴ MD simulations resolve the complete molecular arrangement and describe the evolution of the nano-structured bulk-landscape of ILs, dependent on external agents like temperature, electric fields and pressure.^{25–29} However, DFT/MD simulations are limited due to their computational costs; simulations at length-scales above the nanometer scale are hardly accessible by these atomistic methods.

Continuum theories provide a complementary methodology for dynamic transport simulations of larger systems. Recently, Bazant et al. proposed a phenomenological mean-field-theory for binary ILs at electrified interfaces.³⁰ Using a generalized Landau-Ginzburg functional, the authors show that higher gradients in the electric potential lead to quasi-crystalline structures near electrified interfaces. This finding is confirmed by our theory (see comments below eq. (65)).²¹ Yochelis et al. rationalized this approach, and extended it to bulk phenomena and ternary ILs.^{15–18} Their theoretical work allows fast dynamic simulations but cannot resolve detailed transport processes.

Dilute and concentrated electrolytes for lithium-ion batteries, drive the development of continuum transport theories.³¹ Recently, significant effort was put in the rationalization of consistent theories for neutral-solvent-based electrolytes with high amount of salt.^{19,20,32,33} Although neat ILs constitute the extreme limit of concentrated electrolytes, where the neutral solvent vanishes, such transport theories for lithium ion batteries cannot be generalized to solvent-free electrolytes. This is because ILs exhibit some exceptional behaviour. For example, ILs form characteristic quasi-crystalline structures near electrified interfaces. These extend over a couple of nanometers, which is not observed in regular concentrated electrolytes.³⁴ Our transport theory for ILs, however, also describes stan-

* birger.horstmann@dlr.de

† arnulf.latz@dlr.de

dard electrolytes,³⁵ as the IL-effects decrease under water-dilution,³⁶ or minor additive salts.²¹

Transport theories for highly concentrated electrolytes should contain a condition which prevents ‘‘Coulomb collapse’’ of the ions.³⁷ The prevalent electrostatic attraction can be counteracted by volumetric constraints (‘‘mean steric effects’’) or repulsive particle interactions (‘‘atomistic volumetric exclusion’’). Here, we impose a mean-volume constraint for multicomponent-incompressibility. This results in a threshold for local ion-concentration due to finite volumes. Near electrified interfaces, the concentration-threshold leads to crowding effects.²¹ (Imposing repulsive interactions implies microscopic effects of excluded volume, which lead to overscreening.²¹)

The momentum equation is explicitly used in our derivation. Thereby, we capture the coupling of electric and mechanical stresses in the chemical potentials. This has significant consequences in confined geometries, *e.g.* electrochemical double layers, where volumetric constraints are in strong competition with Coulomb forces.²¹ Electrolyte momentum is given by the center-of-mass convection velocity. Thus, the evolution of convection determines the momentum equation, whereas its variation, expressed by the rate-of-strain, is mandatory for the correct electro-mechanical couplings in the stress tensor. Furthermore, convection is a significant transport-mechanism in solvent-free electrolytes. We take account for these phenomena, derive a convection-equation and consider dissipative, viscous stress in the momentum equation.

We use ILs as validation-template, exemplifying extremely correlated electrolytes. Nevertheless, our theory applies to any liquid multi-component electrolyte, composed of arbitrarily charged (also, neutral) species. Thus it exhibits a very general structure. Our scope of electrolytes includes ILs, IL-salt mixtures, concentrated electrolytes (including aqueous electrolytes) and novel ‘‘water-in-salt’’ electrolytes.³⁸ In particular, for many applications, neat ILs or solutions with high salt-concentrations are supplemented by additives (*e.g.*, water,³⁹ organic solvents,⁴⁰ or salts⁴¹) to improve their performance as electrolytes. The transport theory presented in this work can be tailor-cut to any such heterogeneous mixture.

This article is structured into two main parts. In the first part, we derive our transport theory, which we validate for a zinc-ion battery in the second part.

II. TRANSPORT THEORY

Our transport theory relies on non-equilibrium thermodynamics, supplemented with elements of electromagnetic theory, and mechanics.^{32,42–44} We split this theory-chapter into two sections. In the first section General Transport Theory, we derive the universal framework, which applies to a wide class of systems. We highlight the logical steps of this derivation in four subsections. *First*, we derive the entropy production rate, eq. (15), from the fundamental assumption of conservation of mass, charge, and energy, by formulating the coupled balance equations for momentum, energy and entropy in

section. We use symmetry arguments to guarantee that our model is independent from the state of the observer.^{45,46} Thus, the set of variables is restricted to so-called objective quantities (see section SI 1 A).⁴⁷ Our method applies to a large class of materials and leaves a broad tunability for distinct physical systems. *Second*, we perform our first modeling choices and select a variable-set for strongly correlated electrolytes, eq. (17). Then, we evaluate the entropy production for a general free energy. In the next two steps, we use a linear Onsager-Ansatz to close the system of differential equations. In the *third* subsection, we couple the thermodynamic fluxes and forces, eq. (31), which ensures a positive entropy production. *Fourth*, we assume a linear relationship between viscosity and the velocity-gradients, eq. (49). This determines the model-dependent stress-tensor, eq. (50).

In the second section of this theory-chapter, we specify our framework and model the free energy density for ILs, eq. (52). This casts the specific properties of the medium into the formalism. Here, these properties comprise liquid state, polarizability, temperature dependence, viscosity, and multi-component structure. We further assume incompressibility, and, in the case of bulk transport, electroneutrality. These strong correlations allow to reduce the minimal set of independent variables, eqs. (62) and (63). Finally, we state the equations of motion, eqs. (65) to (69) and (72).

A. General Transport Theory

1. Second Law of Thermodynamics: Entropy

As introduction to our derivation, we present the general structure of a transport theory based on the concepts of non-equilibrium thermodynamics. Our model is implemented as continuum theory for the fundamental physical quantities mass, charge, momentum, energy, and entropy, described by local volume-specific field densities $\psi_A(\mathbf{x})$ at position $\mathbf{x} = (x_1, x_2, x_3)$. We refer to physical quantities with capital letters A, B, C, \dots , to spatial dimensions with lower-case letters i, j, k, \dots , and to dissolved species with Greek letters $\alpha, \beta, \gamma, \dots$. The time evolution of $\psi_A(\mathbf{x})$ is governed by continuity equations,⁴⁸

$$\partial_t \psi_A = \frac{\partial \psi_A}{\partial t} = -\nabla \cdot (\psi_A \otimes \mathbf{v} + \xi_A) + r_A, \quad (1)$$

$$\dot{\psi}_A = \frac{d\psi_A}{dt} = -\psi_A (\nabla \cdot \mathbf{v}) - \nabla \cdot \xi_A + r_A. \quad (2)$$

The partial time derivative $\partial_t \psi_A$ refers to temporal changes in the laboratory system, and the total time derivative $\dot{\psi}_A$ describes temporal changes relative to a co-moving observer at velocity \mathbf{v} . Both are related by a convection term, $\dot{\psi}_A = \partial_t \psi_A + (\mathbf{v} \cdot \nabla) \psi_A$.⁴² The convection velocity \mathbf{v} is defined in the fixed laboratory-frame as center-of-mass average, $\rho \mathbf{v} = \sum_{\alpha=1}^N \rho_\alpha \mathbf{v}_\alpha$, describing bulk electrolyte-momentum per unit mass.

We derive expressions for the production rates r_A and the non-convective flux densities ξ_A for each field variable ψ_A in the remainder of this section.

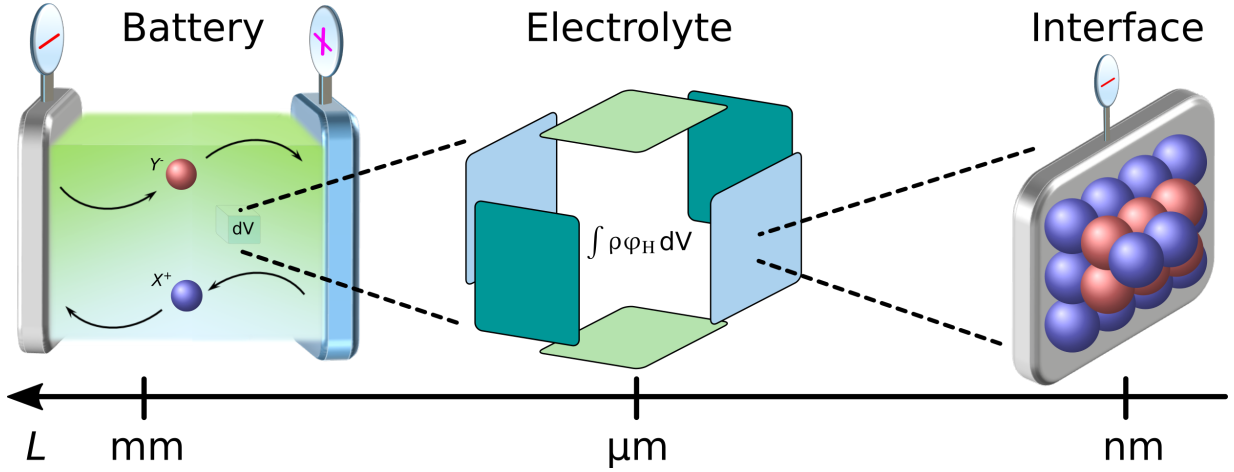


FIG. 1. Scheme of our holistic framework, which captures length-scales from battery-cells to particle interactions. Thus, it describes macroscopic phenomena, like discharging/charging of a battery, mesoscopic effects, like specific electrolyte-dynamics, but also interfacial effects occurring at microscopic scales, like crowding and overscreening.

The total mass density $\rho = \sum_{\alpha=1}^N \rho_{\alpha}$ is conserved in the bulk electrolyte, $\sum_{\alpha=1}^N M_{\alpha} r_{\alpha} = 0$, and it evolves due to convection only,

$$\partial_t \rho = -\nabla \cdot (\rho \mathbf{v}) \quad \text{or} \quad \dot{\rho} = -\rho(\nabla \cdot \mathbf{v}). \quad (3)$$

This special role of the total mass density is used to express the continuity equation 2 in a simpler form

$$\rho \dot{\tilde{\psi}}_A = -\nabla \cdot \tilde{\xi}_A + r_A \quad (4)$$

for the mass-specific field density $\tilde{\psi}_A = \psi_A / \rho$. Individual concentrations c_{α} , however, are affected by non-convective fluxes,

$$\partial_t c_{\alpha} = -\nabla \cdot (c_{\alpha} \mathbf{v} + \mathbf{N}_{\alpha}), \quad (5)$$

$$\dot{c}_{\alpha} = -c_{\alpha} \nabla \cdot \mathbf{v} - \nabla \cdot \mathbf{N}_{\alpha}, \quad (6)$$

where $\mathbf{N}_{\alpha} = c_{\alpha}(\mathbf{v}_{\alpha} - \mathbf{v})$ are the flux densities in the center-of-mass system. We note that these flux densities are related, $\sum_{\alpha=1}^N M_{\alpha} \mathbf{N}_{\alpha} = 0$.

As (total) charge $\varrho = F \sum_{\alpha=1}^N z_{\alpha} c_{\alpha}$ is conserved, we state the balance equation

$$\partial_t \varrho = -\nabla \cdot (\varrho \mathbf{v} + \mathcal{J}) + \sum_{\alpha} F z_{\alpha} r_{\alpha}, \quad (7)$$

where $\mathcal{J} = F \sum_{\alpha=1}^N z_{\alpha} \mathbf{N}_{\alpha}$ is the current density in the center-of-mass system.

Total momentum density $\rho \mathbf{g}$ comprises kinetic and electromagnetic contributions. The correct form of the electromagnetic contribution is under debate in the literature, and various forms have been suggested.⁴⁹ Here, we set $\rho \mathbf{g} = \rho \mathbf{v} + \mathbf{D} \wedge \mathbf{B}$, using the Minkowski-momentum.⁵⁰ We use \mathbf{D} and \mathbf{B} as a Galilei-invariant description of the electromagnetic field, which is consistent with our choice of variables for the free energy density (see eq. (17)). We formulate momentum conservation using Euler's first law of mechanics,

$$\rho \dot{\mathbf{g}} = \nabla \cdot \boldsymbol{\sigma} + \rho \mathbf{b}. \quad (8)$$

Thus, $\rho \mathbf{g}$ changes due to body-forces $\rho \mathbf{b}$ acting upon the system, *e.g.* gravity, and due to anisotropic surface-forces described with the Cauchy-stress tensor $\boldsymbol{\sigma}$. Here, the tensor-gradient is defined as $(\nabla \boldsymbol{\sigma})_i = \sum_{j=1}^3 \partial_j \sigma_{ij}$. We neglect molecular orientations (internal spin) in the isotropic bulk liquid, which implies a symmetric stress tensor, $\boldsymbol{\sigma} = \boldsymbol{\sigma}^T$.⁵¹ In the absence of gravitation, total momentum is conserved, $\rho \mathbf{b} = 0$. Below, we couple energy and momentum balances via body-forces \mathbf{b} . Thus, our derivation proceeds without an explicit model for body-forces.⁵²

The evolution of the energy density ε is determined by work performed on the system,

$$\rho \dot{\varepsilon} = \nabla \cdot (\boldsymbol{\sigma}^T \mathbf{v}) + \rho \mathbf{v} \cdot \mathbf{b} + \rho h - \nabla \cdot \mathbf{q} - \nabla \cdot (\boldsymbol{\mathcal{E}} \wedge \boldsymbol{\mathcal{H}}). \quad (9)$$

The first two terms stem from the non-kinematic mechanical work performed on the system, coupling energy and momentum, see also eq. (8). The third term describes heat production h . As h couples energy and reversible entropy, no constitutive equations for h is needed. This is consistent because heat production, like body-forces \mathbf{b} , is an external field. The last two heat-fluxes are the material heat-flux due to heat-conduction and the momentum-flux of the electromagnetic field, described by the Poynting-vector $\boldsymbol{\mathcal{E}} \wedge \boldsymbol{\mathcal{H}}$. Here, $\boldsymbol{\mathcal{E}} = \mathbf{E} + \mathbf{v} \wedge \mathbf{B}$ and $\boldsymbol{\mathcal{H}} = \mathbf{H} - \mathbf{v} \wedge \mathbf{D}$ are the Galilei-invariant electric and magnetic fields.⁵³

We eliminate the mechanical source-term $\rho \mathbf{v} \cdot \mathbf{b}$ by substitution of eq. (8) into eq. (9). Using the vector identity $\nabla \cdot (\boldsymbol{\sigma}^T \mathbf{v}) = \mathbf{v} \cdot \nabla \boldsymbol{\sigma} + \boldsymbol{\sigma} : \boldsymbol{\kappa}$, we find

$$\rho \dot{\varepsilon} = \boldsymbol{\sigma} : \boldsymbol{\kappa} - \nabla \cdot (\mathbf{q} + \boldsymbol{\mathcal{E}} \wedge \boldsymbol{\mathcal{H}}) + \rho (\mathbf{v} \cdot \mathbf{g} + h). \quad (10)$$

The Cauchy-stress tensor $\boldsymbol{\sigma}$ and the strain-rate-tensor $\boldsymbol{\kappa} = (\text{grad} \mathbf{v} + \text{grad} \mathbf{v}^T)/2$ couple via complete contraction $\boldsymbol{\sigma} : \boldsymbol{\kappa} = \sum_{ij} \sigma_{ij} \kappa_{ij}$. The trace of the strain-rate-tensor, $\text{tr} \boldsymbol{\kappa} = \nabla \cdot \mathbf{v}$, determines volume-expansion, whereas its anti-symmetric part describes shear of the liquid.⁵⁴

According to the second axiom of thermodynamics, entropy is not conserved. We express its evolution with the local

Clausius-Duhem inequality,⁵⁵

$$\rho \dot{s} \geq -\nabla \cdot \boldsymbol{\xi}_s + \frac{\rho h}{T}, \quad (11)$$

where $\boldsymbol{\xi}_s$ is the non-convective entropy flux density. As measure for the deviation from thermodynamic equilibrium, *i.e.*, equality in eq. (11), we define the entropy production rate \mathcal{R} ,

$$\mathcal{R} = \rho T \dot{s} + T \nabla \cdot \boldsymbol{\xi}_s - \rho h \geq 0. \quad (12)$$

Thus, \mathcal{R}/T is the irreversible part of entropy production. We want to find expressions for \mathcal{R} and $\boldsymbol{\xi}_s$. To this aim, we replace the energy production h in the entropy production in eq. (12) with the energy evolution in eq. (10),

$$\mathcal{R} = \rho(T\dot{s} - \dot{u}) + T \nabla \cdot \boldsymbol{\xi}_s - \nabla \cdot \mathbf{q} - \nabla \cdot (\boldsymbol{\mathcal{E}} \wedge \boldsymbol{\mathcal{H}}) + \boldsymbol{\sigma} : \boldsymbol{\kappa} \geq 0. \quad (13)$$

Here, we introduce the internal energy u in the center-of-mass system, and relate it to the total energy ε with the differential relation $\dot{u} = \dot{\varepsilon} - \mathbf{v} \cdot \dot{\mathbf{g}}$.

Our principal modeling-quantity is the free energy density φ_H , which is related to the internal energy u by the Legendre-transformation $\varphi_H = u - Ts$, *i.e.*,

$$\dot{\varphi}_H = \dot{u} - T\dot{s} - \dot{T}s. \quad (14)$$

The Maxwell equations determine the electromagnetic energy flux density, $\nabla \cdot (\boldsymbol{\mathcal{H}} \wedge \boldsymbol{\mathcal{E}}) = \boldsymbol{\mathcal{E}} \cdot \dot{\boldsymbol{\mathcal{J}}} + \boldsymbol{\mathcal{E}} \cdot \dot{\boldsymbol{\mathcal{D}}} + \boldsymbol{\mathcal{H}} \cdot \dot{\boldsymbol{\mathcal{B}}} + [(\boldsymbol{\mathcal{E}} \cdot \dot{\boldsymbol{\mathcal{D}}} + \boldsymbol{\mathcal{H}} \cdot \dot{\boldsymbol{\mathcal{B}}}) \mathbf{Id} - \boldsymbol{\mathcal{E}} \otimes \dot{\boldsymbol{\mathcal{D}}} - \boldsymbol{\mathcal{H}} \otimes \dot{\boldsymbol{\mathcal{B}}}] : \text{grad } \mathbf{v}$, see section SI 1 B. Thus, the entropy production rate becomes

$$\mathcal{R} = -\rho \dot{\varphi}_H - \rho s \dot{T} + T \nabla \cdot \boldsymbol{\xi}_s - \nabla \cdot \mathbf{q} + \boldsymbol{\mathcal{E}} \cdot \dot{\boldsymbol{\mathcal{J}}} + \boldsymbol{\mathcal{E}} \cdot \dot{\boldsymbol{\mathcal{D}}} + \boldsymbol{\mathcal{H}} \cdot \dot{\boldsymbol{\mathcal{B}}} + [\boldsymbol{\sigma} + (\boldsymbol{\mathcal{E}} \cdot \dot{\boldsymbol{\mathcal{D}}} + \boldsymbol{\mathcal{H}} \cdot \dot{\boldsymbol{\mathcal{B}}}) \mathbf{Id} - \boldsymbol{\mathcal{E}} \otimes \dot{\boldsymbol{\mathcal{D}}} - \boldsymbol{\mathcal{H}} \otimes \dot{\boldsymbol{\mathcal{B}}}] : \text{grad } \mathbf{v} \geq 0. \quad (15)$$

We continue evaluating the entropy production \mathcal{R} , and the entropy flux density $\boldsymbol{\xi}_s$ by modeling the free energy density φ_H in the next section. The final form of \mathcal{R} then describes dissipative processes and determines our transport equations.

2. First Law Of Thermodynamics: Energy

The discussions above are valid for many materials.⁴⁴ In this section, we describe the process of modeling material properties and derive constitutive equations for the field variables.

The Helmholtz free energy F is the focal point of our material model. In this work, we study bulk-phenomena and model the corresponding local free energy density φ_H ,

$$F = \int_V \rho \varphi_H dV. \quad (16)$$

Nevertheless, our theory can be extended to non-local phenomena which are important at electrochemical interfaces. For example, we have recently shown how to supplement F with an interaction-functional, incorporating the particle-nature of the constituents.²¹ For a multi-component, polarizable and magnetizable liquid,⁴⁹ the total differential of the free

energy density reads

$$d(\rho \varphi_H) = \boldsymbol{\mathcal{E}} \cdot d\mathbf{D} + \boldsymbol{\mathcal{H}} \cdot d\mathbf{B} - \rho s \cdot dT + \sum_{\alpha=1}^N \mu_\alpha \cdot dc_\alpha. \quad (17)$$

Temperature T and concentrations c_α are varied according to standard thermodynamics.³² The differential energy $\boldsymbol{\mathcal{E}} \cdot d\mathbf{D} + \boldsymbol{\mathcal{H}} \cdot d\mathbf{B}$ with the independent, Galilei invariant variables \mathbf{D} and \mathbf{B} is valid for linear and non-linear materials.⁵⁶ Previous works, however, have chosen $\boldsymbol{\mathcal{E}}^2$ or (\mathbf{P}, \mathbf{M}) ³² as independent variables. Since only unique transformations between the electromagnetic variables exist, this poses no problem,⁵⁷ but leads to different expressions for the stress-tensors and the body-forces employed in the balance-laws.⁵² Varying the free energy density with respect to the strain-tensor would extend the model to (visco)-elastic materials, which lies beyond the scope of this work.

This total differential in eq. (17) consists of products $X^A \cdot d\gamma^A$, where X^A describes a particular reaction of the medium subject to variations of the external quantity γ^A . This motivates using $\boldsymbol{\mathcal{Y}} = \{\gamma^A\}$ as variable-set for F and φ_H . However, the variational expansion of the free energy does not capture the complete variable-set, as it does not comprise viscous, dissipative effects. In particular, viscous liquids cannot sustain shear stress (unlike elastic media) and depend on the rate of strain. Due to symmetry-arguments (see section SI 1 A), we use the symmetrized, objective strain rate tensor.^{58–60} Thus, we model electrolytes with the objective variable set $\boldsymbol{\mathcal{Y}} = \{T, c_\alpha, \mathbf{D}, \mathbf{B}, \boldsymbol{\kappa}\}$.

The variation of free energy density in eq. (17) contains some constitutive equations,

$$s = -\frac{\partial \varphi_H}{\partial T}, \quad (18)$$

$$\boldsymbol{\mathcal{E}} = \rho \frac{\partial \varphi_H}{\partial \mathbf{D}}, \quad (19)$$

$$\boldsymbol{\mathcal{H}} = \rho \frac{\partial \varphi_H}{\partial \mathbf{B}}, \quad (20)$$

$$\mu_\alpha = \frac{\partial(\rho \varphi_H)}{\partial c_\alpha}. \quad (21)$$

These are supplemented by $\partial(\rho \varphi_H)/\partial \kappa_{ij} = 0$. Equation (18) implies a constitutive equation for the internal energy density, $\rho u = -T^2 \cdot \partial/\partial T(\rho \varphi_H/T)$. Constitutive equations relate conjugate variable-pairs, (s, T) , $(\boldsymbol{\mathcal{E}}, \mathbf{D})$, $(\mu_\alpha, \rho_\alpha)$, $(\boldsymbol{\mathcal{H}}, \mathbf{B})$ and thus complement the universal balance equations with material-specific properties.

We want to determine $\rho \dot{\varphi}_H$ as it enters the entropy production \mathcal{R} in eq. (15). To this aim, the standard method of Coleman and Noll,⁴² assumes $\dot{\varphi}_H(\boldsymbol{\mathcal{Y}}) = \sum_A \partial \varphi_H / \partial \gamma^A \cdot \dot{\gamma}^A$. However, this expansion would result in ambiguous constitutive equations for the chemical potentials because the variable-set $\boldsymbol{\mathcal{Y}}$ is not independent and contains redundancies (see section SI 1 D). Instead, we determine $\rho \dot{\varphi}_H$ from the total differential of the free energy density (see eq. (17)),

$$\rho \dot{\varphi}_H = \frac{d(\rho \varphi_H)}{dt} - \dot{\rho} \varphi_H = \frac{d(\rho \varphi_H)}{dt} + \rho \varphi_H \nabla \cdot \mathbf{v}$$

$$= \mathcal{E}\mathbf{D} + \mathcal{H}\mathbf{B} - \rho s\dot{T} + \sum_{\alpha} \mu_{\alpha} \dot{c}_{\alpha} + \rho \varphi_{\text{H}} \nabla \mathbf{v}, \quad (22)$$

where we use the mass continuity equation (see eq. (3)). Replacing the concentration change \dot{c}_{α} with the mass balance eq. (5) and using $\nabla \mathbf{v} = \mathbf{Id} : \boldsymbol{\kappa}$, we identify the entropy flux density,⁴⁴

$$\boldsymbol{\xi}_s = \frac{1}{T} (\mathbf{q} - \mu_{\alpha} \mathbf{N}_{\alpha}), \quad (23)$$

and the entropy production rate,

$$\mathcal{R} = \boldsymbol{\tau} : \boldsymbol{\kappa} - \boldsymbol{\xi}_s \nabla T - \mathcal{J} \nabla \Phi - \sum_{\alpha=1}^N \mathbf{N}_{\alpha} \nabla \mu_{\alpha}, \quad (24)$$

with the symmetric viscosity tensor $\boldsymbol{\tau}(\boldsymbol{\gamma}) = \boldsymbol{\sigma} - (\mathcal{E} \otimes \mathbf{D} + \mathcal{H} \otimes \mathbf{B}) + (\mathcal{E}\mathbf{D} + \mathcal{H}\mathbf{B} + \sum_{\alpha=1}^N \mu_{\alpha} c_{\alpha} - \rho \varphi_{\text{H}}) \mathbf{Id}$. To derive eq. (24), we use that $\mathcal{E} \otimes \mathbf{D}$ and $\mathcal{H} \otimes \mathbf{B}$ is symmetric, see section SI 1 C.

The entropy production rate \mathcal{R} comprises correlations between thermodynamic forces and thermodynamic potentials, $\mathbf{N}_{\alpha} \nabla \mu_{\alpha}$, $\mathcal{J} \nabla \Phi$ and $\boldsymbol{\xi}_s \nabla T$. Positivity of \mathcal{R} constitutes an important role in our framework, constraining the generalized fluxes. We proceed by determining the fluxes \mathbf{N}_{α} , $\boldsymbol{\xi}_s$, and the stress tensor $\boldsymbol{\sigma}$ in the next two paragraphs, see eqs. (43), (44), (46) and (50).

3. Flux Densities

In this section, we determine the flux densities \mathbf{N}_{α} , $\boldsymbol{\xi}_s$ relative to the center-of-mass velocity using the Onsager-formalism.⁴³ This relates the transport equations to the modeled free energy density φ_{H} .

A dimensional analysis of the Maxwell-equations reveals that magnetic effects in the bulk-electrolyte can be neglected under normal operating conditions of electrochemical systems.³² We thus assume from now on the electrostatic limit ($\mathbf{B} = 0$), and introduce the electric potential Φ such that $\mathcal{E} = \mathbf{E} = -\nabla \Phi$.

Using center-of-mass convection as reference velocity in our transport theory implies that the trivial flux-constraint

$$\sum_{\alpha=1}^N M_{\alpha} \cdot \mathbf{N}_{\alpha} = 0, \quad (25)$$

emerges naturally. Thus, only $N-1$ such fluxes \mathbf{N}_{α} are independent, and eq. (25) requires to reduce the number of species. To this aim, we define reduced valences and chemical potentials with respect to the designated species $\alpha = 1$,

$$\tilde{z}_{\alpha} = z_{\alpha} - z_1 \cdot \frac{M_{\alpha}}{M_1}, \quad (26)$$

$$\tilde{\mu}_{\alpha} = \mu_{\alpha} - \mu_1 \cdot \frac{M_{\alpha}}{M_1}. \quad (27)$$

In the validation chapter, we demonstrate that the predictions of our theory, if applied correctly, are independent of the

choice of the designated species. This reduction can lead to counter-intuitive contributions to the electric current,

$$\mathcal{J} = F \sum_{\alpha=2}^N \tilde{z}_{\alpha} \cdot \mathbf{N}_{\alpha}. \quad (28)$$

By construction, $\tilde{z}_1 = 0$. Thus the designated species does not contribute, even if it is charged, $z_1 \neq 0$. Furthermore, if the designated species is charged, $z_1 \neq 0$, then even neutral species carry effective charge and contribute to \mathcal{J} . This is one reason behind recent confusion with respect to solvent-free electrolytes, *e.g.*, molten-salts,^{61,62} and ILs.^{63,64} For electrolytes with neutral solvents, the natural choice for the designated species is the solvent,²⁰ since then $\tilde{z}_{\alpha} = z_{\alpha}$.

The entropy production rate in the reduced formalism becomes

$$\mathcal{R} = \boldsymbol{\tau} : \boldsymbol{\kappa} - \sum_{\alpha=2}^N \mathbf{N}_{\alpha} (F \tilde{z}_{\alpha} \nabla \Phi + \nabla \tilde{\mu}_{\alpha}) - \boldsymbol{\xi}_s \nabla T \quad (29)$$

$$= \boldsymbol{\tau} : \boldsymbol{\kappa} - \sum_{(a)} \boldsymbol{\Psi}_{(a)} \cdot \mathbf{X}_{(a)} \geq 0. \quad (30)$$

Here, we defined the vector of thermodynamic forces $\mathbf{X}_{(a)} = (F \tilde{z}_{\alpha} \nabla \Phi + \nabla \tilde{\mu}_{\alpha}, \nabla T)$ and the vector of thermodynamic fluxes $\boldsymbol{\Psi}_{(a)} = (\mathbf{N}_{\alpha}, \boldsymbol{\xi}_s)$ with components $\Psi_{(a)}^A$. The subscripts in brackets denote that only the ionic contributions are species-related.

We make use of this expansion and transfer the products to quadratic terms via a bilinear Onsager-matrix. Thus, this Onsager formalism (i) closes the system of equations, (ii) establishes positivity of \mathcal{R} , and (iii) evaluates the flux-force couplings. The phenomenological relations linearly couple thermodynamic fluxes and forces with the Onsager matrix $\mathcal{L}_{(a)(\beta)}$,

$$\boldsymbol{\Psi}_{(a)}^A = - \sum_{\beta=2}^N \mathcal{L}_{(a)(\beta)} \mathbf{X}_{(\beta)}, \quad (31)$$

$$\begin{pmatrix} \mathbf{N}_2 \\ \vdots \\ \mathbf{N}_N \\ \boldsymbol{\xi}_s \end{pmatrix} = - \begin{pmatrix} \mathcal{L}_{22} & \dots & \mathcal{L}_{2N} & \mathcal{L}_{2T} \\ \vdots & \ddots & \vdots & \vdots \\ \mathcal{L}_{2N} & \dots & \mathcal{L}_{NN} & \mathcal{L}_{NT} \\ \mathcal{L}_{2T} & \dots & \mathcal{L}_{NT} & \mathcal{L}_{TT} \end{pmatrix} \cdot \begin{pmatrix} F \tilde{z}_2 \nabla \Phi + \nabla \tilde{\mu}_2 \\ \vdots \\ F \tilde{z}_N \nabla \Phi + \nabla \tilde{\mu}_N \\ \nabla T \end{pmatrix}. \quad (32)$$

The Onsager matrix $\mathcal{L}_{(a)(\beta)}$ is symmetric and positive semi-definite.⁶⁵ This guarantees that the corresponding term in the entropy production rate \mathcal{R} is always positive (see eq. (30)). Thus, electrolyte transport is a dissipative process, which wants to equilibrate the system. In dilute solutions, the Onsager matrix is diagonal and describes intra-species correlations. In concentrated electrolytes, off-diagonal Onsager coefficients comprise inter-species correlations, *e.g.*, electro-osmotic drag through a membrane⁶⁶ or asymmetric transference numbers.⁶⁷ In total, we define $N(N+1)/2$ independent Onsager coefficients, *i.e.*, transport parameters.

The thermodynamic fluxes are driven by electric potential gradients, concentration gradients, and temperature gradients, *i.e.*, migration, diffusion, and thermo-electric effects. In the following, we relate the abstract Onsager coefficients to these

physico-chemical effects. The electric current density \mathcal{J} (see eq. (28)) is expressed as

$$\mathcal{J} = -\kappa \nabla \Phi - \kappa \sum_{\beta=2}^N \frac{t_\beta}{F \tilde{z}_\beta} \nabla \tilde{\mu}_\beta - \kappa \beta \nabla T. \quad (33)$$

The flux densities \mathbf{N}_α and the entropy flux density ξ_s are often formulated in terms of \mathcal{J} instead of Φ . Therefore, we transform eq. (32) by substituting $\nabla \Phi$ for \mathcal{J} with eq. (33) and introducing additional, physically motivated parameters,

$$\mathbf{N}_\alpha = \frac{t_\alpha \mathcal{J}}{F \tilde{z}_\alpha} - \sum_{\beta=2}^N \left(\mathcal{L}_{\alpha\beta} - \frac{\kappa t_\alpha t_\beta}{F^2 \tilde{z}_\alpha \tilde{z}_\beta} \right) \nabla \tilde{\mu}_\beta - \left(\mathcal{L}_{\alpha T} - \frac{\beta \kappa t_\alpha}{F \tilde{z}_\alpha} \right) \nabla T, \quad (34)$$

$$\xi_s = \beta \mathcal{J} - \left(\frac{\gamma}{T} - \beta^2 \kappa \right) \nabla T - \sum_{\beta=2}^N \left(\mathcal{L}_{\beta T} - \beta \frac{\kappa t_\beta}{F \tilde{z}_\beta} \right) \nabla \tilde{\mu}_\beta. \quad (35)$$

Transport coefficients introduced in eqs. (33), (34) and (35) are electric conductivity κ , Seebeck coefficient β , and thermal conductivity γ ,³¹

$$\kappa = F^2 \sum_{\alpha, \beta=2}^N \mathcal{L}_{\alpha\beta} \tilde{z}_\alpha \tilde{z}_\beta, \quad (36)$$

$$\beta = \frac{F}{\kappa} \sum_{\alpha=2}^N \mathcal{L}_{\alpha T} \tilde{z}_\alpha, \quad (37)$$

$$\gamma = T \mathcal{L}_{TT}. \quad (38)$$

By construction, κ and γ are positive because the Onsager matrix is positive semi-definite. N-1 transference numbers t_α relate particle fluxes and electric current in eq. (34),

$$t_\alpha = \frac{F^2 \tilde{z}_\alpha}{\kappa} \sum_{\beta=2}^N \mathcal{L}_{\alpha\beta} \tilde{z}_\beta. \quad (39)$$

These N-1 parameters are subject to the normalization condition, $\sum_{\alpha=2}^N t_\alpha = 1$, such that only N-2 transference numbers are independent. Thus, for binary electrolytes all transference numbers are fixed, $t_2^{N=2} = 1$, and \mathbf{N}_1 relates to \mathcal{J} by the specific mass-ratio alone, see section SI I H. Apparently, all t_α are positive if the Onsager matrix is diagonal (as for dilute solutions).

We proceed by defining the $N(N+1)/2$ coefficients of the symmetric diffusion matrix \mathcal{D} ,

$$\begin{aligned} \mathcal{D}_{\alpha\beta} &= \mathcal{L}_{\alpha\beta} - \frac{\kappa t_\alpha t_\beta}{F^2 \tilde{z}_\alpha \tilde{z}_\beta}, \\ \mathcal{D}_{\alpha T} &= \mathcal{L}_{\alpha T} - \frac{\beta \kappa t_\alpha}{F \tilde{z}_\alpha}, \\ \mathcal{D}_{TT} &= \frac{\gamma}{T} - \beta^2 \kappa. \end{aligned} \quad (40)$$

Since \mathcal{D}_{TT} is determined by γ , β and κ , eqs. (36) to (40) yield $N(N+3)/2$ transport coefficients. Thus, the number of transport parameters defined so far exceeds the number of independent Onsager coefficients $N(N+1)/2$. However, further N

constraints follow from the relation of \mathcal{J} and \mathbf{N}_α in eq. (28),

$$\sum_{\beta=2}^N \mathcal{D}_{\alpha\beta} \tilde{z}_\beta = 0, \quad \sum_{\beta=2}^N \mathcal{D}_{T\beta} \tilde{z}_\beta = 0, \quad (41)$$

Thus, only $N(N-1)/2$ diffusion coefficients are independent, where $\mathcal{D}_{2\alpha} = -\sum_{\beta=3}^N \mathcal{D}_{\alpha\beta} \tilde{z}_\beta / \tilde{z}_2$ and $\mathcal{D}_{2T} = -\sum_{\beta=3}^N \mathcal{D}_{T\beta} \tilde{z}_\beta / \tilde{z}_2$. In particular $\mathcal{D}_{22} = \sum_{\beta, \gamma=3}^N \mathcal{D}_{\beta\gamma} \tilde{z}_\beta \tilde{z}_\gamma / (\tilde{z}_2)^2$. Altogether, $N(N-1)/2$ independent diffusion coefficients, N-2 independent transference numbers, the electric conductivity, and the Seebeck coefficient constitute the complete set of physically motivated free parameters.

We designate a second species, $\alpha = 2$, and define the set of N-2 reduced chemical potentials

$$\tilde{\mu}_\beta = \tilde{\mu}_\beta - \frac{\tilde{z}_\beta}{\tilde{z}_2} \cdot \tilde{\mu}_2. \quad (42)$$

Thus N-1 independent fluxes ($\mathbf{N}_3, \dots, \mathbf{N}_N, \xi_s$) exist,

$$\mathbf{N}_\alpha = \frac{t_\alpha}{F \tilde{z}_\alpha} \mathcal{J} - \mathcal{D}_{\alpha T} \nabla T - \sum_{\beta=3}^N \mathcal{D}_{\alpha\beta} \nabla \tilde{\mu}_\beta, \quad \alpha \geq 3 \quad (43)$$

$$\xi_s = \beta \mathcal{J} - \mathcal{D}_{TT} \nabla T - \sum_{\beta=3}^N \mathcal{D}_{\beta T} \nabla \tilde{\mu}_\beta. \quad (44)$$

\mathbf{N}_2 is determined by the electric flux with eq. (28) and \mathbf{N}_1 is determined by mass conservation in eq. (25). Our electrolyte potential Φ is the Maxwell potential that appears in the Poisson equation. Typically,^{20,31} concentrated solution theory is expressed using the alternative potential

$$\varphi(\Phi, \mu_{1,2}, M_{1,2}, z_{1,2}) = \Phi + \tilde{\mu}_2 / F \tilde{z}_2. \quad (45)$$

If the first designated species is the neutral solvent, $\varphi = \Phi + \tilde{\mu}_2 / F \tilde{z}_2$ corresponds to the electro-chemical potential of the second designated species. With the electrolyte potential φ , we can express the current density analogous to eq. (43) and eq. (44),

$$\mathcal{J} = -\kappa \nabla \varphi - \beta \kappa \nabla T - \frac{\kappa}{F} \sum_{\beta=3}^N \frac{t_\beta}{\tilde{z}_\beta} \nabla \tilde{\mu}_\beta. \quad (46)$$

The entropy production rate \mathcal{R} in the double reduced formalism is

$$\begin{aligned} \mathcal{R} &= \boldsymbol{\tau} : \boldsymbol{\kappa} - \mathcal{J} \nabla \varphi - \sum_{\alpha=3}^N \mathbf{N}_\alpha \nabla \tilde{\mu}_\alpha - \xi_s \nabla T \\ &= \boldsymbol{\tau} : \boldsymbol{\kappa} + \mathcal{J}^2 / \kappa + \\ &\quad + (\nabla \tilde{\mu}_3, \dots, \nabla \tilde{\mu}_N, \nabla T) \cdot \mathcal{D}_{(\alpha),(\beta)}^{\text{red}} \cdot (\nabla \tilde{\mu}_3, \dots, \nabla \tilde{\mu}_N, \nabla T)^T \\ &\geq 0, \end{aligned} \quad (47)$$

where \mathcal{D}^{red} is the diffusion matrix \mathcal{D} without the two designated species (see eq. (40)). To summarize, the entropy production comprises three contributions. The first term describes mechanical dissipation. In the next paragraph, we determine $\boldsymbol{\tau}$ in such a way that $\boldsymbol{\tau} : \boldsymbol{\kappa} \geq 0$ is guaranteed. The

second term describes Joule-heating due to migration. Since the electric conductivity is non-negative, $\mathcal{J}^2/\kappa \geq 0$. The last term describes entropy production due to diffusion and heat conduction. Thermodynamic consistency reduces to non-negativity of the diffusion matrix, $\mathcal{D}^{\text{red}} \geq 0$.

4. Stress Tensor

In contrast to viscous-elastic models, this description does not describe the stress tensor by a constitutive equation in the form of a derivative of the free energy density.^{44,68} Instead, we determine $\boldsymbol{\sigma}$ implicitly via the viscosity tensor. To find $\boldsymbol{\tau}(\boldsymbol{\kappa})$, we apply the Onsager formalism as in the previous subsection, and assume that $\boldsymbol{\tau}$ is linear in the strain-rate tensor. Symmetry demands that $\boldsymbol{\tau}$ is an objective tensor, thus the representation theorems for isotropic tensors determine it uniquely up to two scalar transport parameters of viscosity,^{69,70}

$$\boldsymbol{\tau} = \lambda(T, \rho_\alpha)(\nabla \mathbf{v}) \mathbf{Id} + 2\eta(T, \rho_\alpha)\boldsymbol{\kappa}_{\text{tf}}, \quad (48)$$

where $\boldsymbol{\kappa}_{\text{tf}}$ is the *symmetric* trace-free part of $\boldsymbol{\kappa}$, λ is the bulk-viscosity and η is the shear-viscosity. Since

$$\boldsymbol{\tau} : \boldsymbol{\kappa} = \lambda(\nabla \mathbf{v})^2 + 2\eta\boldsymbol{\kappa}_{\text{tf}} : \boldsymbol{\kappa}_{\text{tf}} \geq 0, \quad (49)$$

the entropy production rate \mathcal{R} is non-negative (see eq. (24)), if the viscosities obey $\eta \geq 0$ and $\lambda \geq 0$. To summarize, we find as constitutive equation for the *symmetric* stress tensor,⁷¹

$$\boldsymbol{\sigma} = \mathbf{E} \otimes \mathbf{D} + \left(\rho\varphi_{\text{H}} - \sum_{\alpha=1}^N c_\alpha \mu_\alpha - \mathbf{E} \mathbf{D} + \lambda \nabla \mathbf{v} \right) \mathbf{Id} + 2\eta\boldsymbol{\kappa}_{\text{tf}}. \quad (50)$$

The pressure p measured in experiments is derived from the total stress tensor,^{32,72}

$$p = -\frac{1}{3}\text{tr}(\boldsymbol{\sigma}) = p^{\text{td}} - \lambda \cdot \nabla \mathbf{v}. \quad (51)$$

Here, $p^{\text{td}} = \sum_{\alpha=1}^N c_\alpha \mu_\alpha - \rho\varphi_{\text{H}} + 2\mathbf{E} \mathbf{D}/3$ is the thermodynamic pressure comprising the standard Gibbs-Duhem contribution, and a Maxwell-contribution. The further contribution, $\lambda \nabla \mathbf{v}$, describes dissipation due to friction. Since $\lambda \geq 0$, friction can lead to positive and negative pressures, depending on $\nabla \mathbf{v}$.

The apparent electromagnetic contribution to the total stress $\boldsymbol{\sigma}$ in eq. (50) differs from the Maxwell contribution $\boldsymbol{\Sigma} = -\mathbf{E} \mathbf{D}/2 + \mathbf{E} \otimes \mathbf{D}$. Note that we recover the correct standard form once we model and specify φ_{H} (see eq. (54)).

B. Model for Correlated Liquid Electrolytes

The transport equations of any electrolyte-model depend on the specific form of the free energy density φ_{H} . In our approach, φ_{H} is the focal point of modeling. Once φ_{H} is specified, all equations follow from plain mathematics. In this section we introduce our model φ_{H} , derive the convection velocity from the volumetric electrolyte equation of state, and discuss the dynamic transport equations.

1. Free Energy Density

As discussed in the previous section, we assume that the free energy density φ_{H} depends on temperature T , concentrations c_α , and dielectric displacement \mathbf{D} (see eq. (17) and the discussion thereafter).^{20,32} Our model for liquid electrolytes is generated by

$$\rho\varphi_{\text{H}} = \frac{\mathbf{D}^2}{2\varepsilon_0(1+\chi)} + \frac{\mathcal{K}}{2} \left(1 - \sum_{\alpha=1}^N v_\alpha^0 c_\alpha \right)^2 + RT \sum_{\alpha=1}^N c_\alpha \ln \left(\frac{c_\alpha}{c} \right) + \rho\varphi_{\text{H}}^{\text{int}}. \quad (52)$$

The first term comprises the electrostatic energy-density of polarizable media.⁵⁶ The electric field follows from eq. (19), $\mathbf{E} = \mathbf{D}/\varepsilon_0(1+\chi)$, which describes a linear dielectric medium. We neglect the dependence of susceptibility χ on ion composition such that the chemical potentials do not depend on dielectric displacement (see section SI I I I).

The second term expresses volumetric contributions with partial molar volumes v_α^0 in a stable reference state, which couple to surface forces acting upon the system. These surface forces are usually expressed by pressure (see eq. (54)). Here, \mathcal{K} is the bulk-modulus which acts as a Lagrange-mutliplier in the case of incompressible electrolytes (see eq. (59)). We expand the energy of deformations around a stable reference state in order to easily transfer to incompressible media, see eq. (59). These volumetric energy penalties encode volume conservation (see eq. (57)), and account for mean steric effects,¹⁴ which are crucial for continuum theories of concentrated electrolytes⁷³ and ILs.¹⁶ Mean steric effects create a threshold for local ion-concentration and prevent Coulombic collapse of the system.³⁷ This leads to crowding of ILs near electrified interfaces.²¹ We motivate this expression for the elastic energy in the supplementary (section SI I F).

The third term is the entropy of mixture for non-interacting systems. We model this term in analogy with ideal gases and neglect contributions from inter-molecular interactions, *e.g.*, solvation effects.

We phenomenologically account for non-ideal interaction contributions in $\rho\varphi_{\text{H}}^{\text{int}}$. The activity-coefficients f_α measure the deviation from ideal/dilute electrolytes ($f_\alpha c = 1$) via $\partial(\rho\varphi_{\text{H}}^{\text{int}})/\partial c_\alpha = RT \ln(f_\alpha c)$. The interaction term $\rho\varphi_{\text{H}}^{\text{int}}$ can also describe the heat capacity of the system, $\mathcal{C} = -T \cdot \partial^2(\rho\varphi_{\text{H}}^{\text{int}})/\partial T^2$. Since thermal aspects are not our main focus, we refer to the supplementary for a thermal contribution to our free energy model $\rho\varphi_{\text{H}}$ (section SI I I 3).

In the following, we calculate the chemical potentials μ_α and the stress tensor from the model free energy density in eq. (52). The chemical potentials follow by evaluation of the constitutive eq. (21),

$$\mu_\alpha = RT \ln(f_\alpha c_\alpha) - \mathcal{K} v_\alpha^0 \left(1 - \sum_{\beta=1}^N v_\beta^0 c_\beta \right). \quad (53)$$

The first term comprises entropy of mixture and inter-molecular interaction energies. The stress tensor is determined by

eq. (50),

$$\boldsymbol{\sigma} = \mathbf{E} \otimes \mathbf{D} - \frac{\mathbf{E}\mathbf{D}}{2} \mathbf{Id} + \frac{\mathcal{K}}{2} \mathbf{Id} - \frac{\mathcal{K}}{2} \left(\sum_{\alpha=1}^N c_{\alpha} \nu_{\alpha}^0 \right)^2 \mathbf{Id} + \lambda \cdot \nabla \mathbf{v} \mathbf{Id} + 2\eta \boldsymbol{\kappa}_{\text{tf}} - \rho \sum_{\alpha=1}^N c_{\alpha} \frac{\partial \varphi_{\text{H}}^{\text{int}}}{\partial c_{\alpha}} \mathbf{Id}. \quad (54)$$

Thus, the electrostatic contribution is the expected electrostatic Maxwell-stress tensor $\boldsymbol{\Sigma}$.⁵⁶ The elastic stress due to compressibility and the stress due to intra-molecular interaction is also diagonal, *i.e.*, isotropic. Shear stress due to viscosity contains the non-isotropic contribution $2\eta \boldsymbol{\kappa}_{\text{tf}}$.

2. Volume Constraint and Convection

In this section, we derive the equation of state for liquids from our model free energy (see eq. (52)), and discuss incompressibility of electrolytes. In addition, we derive a multi-component incompressibility constraint, and a transport equation for the center-of-mass convection velocity \mathbf{v} .

In a homogeneous system we neglect viscosity. In this case $p = p^{\text{id}}$ becomes the thermodynamic pressure as discussed for (51). Equation (54) determines,

$$p = p^{\text{id}} = -\text{tr}(\boldsymbol{\sigma}|_{\nabla \mathbf{v}=0})/3 = f(c_{\alpha}, T, \mathbf{D}), \quad (55)$$

as a function of c_{α} , T , and \mathbf{D} . This expression implicitly determines volume $V(\mathcal{N}_{\alpha}, p, T, \mathbf{D})$ as function of particle numbers \mathcal{N}_{α} , pressure p , temperature T , and dielectric displacement \mathbf{D} . We make use of this description, and define partial molar volumes ν_{α} as derivative of V with respect to \mathcal{N}_{α} . Implicit differentiation of the function $f(c_{\alpha}, T, \mathbf{D})$ then determines the partial molar volumes (see section **SI 1 E**),

$$\nu_{\alpha} = \frac{\partial V}{\partial \mathcal{N}_{\alpha}} \Big|_{T,p,\mathbf{D}} = \frac{\partial f / \partial c_{\alpha}}{\sum_{\beta=1}^N \partial f / \partial c_{\beta} \cdot c_{\beta}} \Big|_{T,p,\mathbf{D}}. \quad (56)$$

Thus, the partial molar volumes of the electrolyte follow from the stress tensor.

As $V(\mathcal{N}_{\alpha}, p, T, \mathbf{D})$ is a homogeneous function of first order in \mathcal{N}_{β} , Euler's homogeneous function theorem yields a compact form of the electrolyte equation of state of liquid electrolytes,^{16,73–76}

$$V = \sum_{\alpha=1}^N \nu_{\alpha} \mathcal{N}_{\alpha} \quad \text{or} \quad 1 = \sum_{\alpha=1}^N \nu_{\alpha} c_{\alpha}, \quad (57)$$

which takes the form of a volume constraint.

From eq. (56), we calculate the partial molar volumes for our model. Liquid electrolytes are hardly compressible, *i.e.*, $\mathcal{K} \gg p$. Repeated application of this approximation yields

$$\nu_{\alpha} \approx \frac{\nu_{\alpha}^0}{\sum_{\beta=1}^N \nu_{\beta}^0 c_{\beta}} \quad (58)$$

$$\approx \nu_{\alpha}^0 - \frac{\nu_{\alpha}^0}{\mathcal{K}} \left(p - \frac{\mathbf{E}\mathbf{D}}{6} - \rho \sum_{\alpha=1}^N c_{\alpha} \frac{\partial \varphi_{\text{H}}^{\text{int}}}{\partial c_{\alpha}} \right). \quad (59)$$

Here, we used eq. (55) and eq. (54) to replace $\sum_{\beta=1}^N \nu_{\beta}^0 c_{\beta}$. Thus, \mathcal{K} is indeed the bulk-modulus, and ν_{α}^0 is the partial molar volume at standard pressure $p = 0$. For incompressible electrolytes $\mathcal{K} \rightarrow \infty$, the partial molar volumes $\nu_{\alpha} = \nu_{\alpha}^0$ do not depend on pressure, and eq. (57) constitutes an incompressibility constraint.²¹ In this case, pressure cannot be determined by eq. (55). Nevertheless, the volumetric contributions in the chemical potentials have to be determined (see eq. (53)). We show in eq. (65), how to solve this challenge with the volumetric contributions in the stress-tensor and momentum conservation.

The volume constraint in eq. (57) remains fulfilled under multi-component transport as the center-of-mass motion balances the volumes. Thus, we can derive an equation for the velocity \mathbf{v} from the volume constraint. To this aim, let us first prove a Lemma. Partial molar volumes ν_{α} defined in eq. (56) obey the symmetry-property $\partial \nu_{\alpha} / \partial \mathcal{N}_{\beta} = \partial \nu_{\beta} / \partial \mathcal{N}_{\alpha}$. Applying Euler's homogeneous function theorem to ν_{α} ensures that $\sum_{\beta=1}^N c_{\beta} \partial \nu_{\alpha} / \partial \mathcal{N}_{\beta} = 0$ holds for all species. These relations prove the following Lemma,

$$\sum_{\alpha=1}^N c_{\alpha} \dot{\nu}_{\alpha} = \sum_{\alpha=1}^N \frac{\partial (c_{\alpha} \nu_{\alpha})}{\partial T} \cdot \dot{T} + \sum_{\alpha=1}^N \sum_{\beta=1}^N c_{\alpha} \frac{\partial \nu_{\alpha}}{\partial \mathcal{N}_{\beta}} \cdot \dot{\mathcal{N}}_{\beta} = 0, \quad (60)$$

where we used the independence of the primary variables c_{α} , T and the volume constraint.

Applying the total time derivative to the volume constraint in eq. (57), we conclude from our Lemma that $\sum_{\alpha=1}^N \dot{c}_{\alpha} \nu_{\alpha} = 0$. In combination with mass conservation eq. (5) for the concentrations c_{α} , we finally derive the equation for the center-of-mass velocity \mathbf{v} ,^{35,77,78}

$$\nabla \mathbf{v} = - \sum_{\alpha=1}^N \nu_{\alpha} \nabla \mathcal{N}_{\alpha} + \sum_{\alpha=1}^N \nu_{\alpha} r_{\alpha}. \quad (61)$$

This equation is generally true for compressible as well as incompressible electrolytes and for constant as well as non-constant partial molar volumes.

The left-hand side of eq. (61) expresses local, isotropic volume-expansion, $\nabla \mathbf{v} = \text{tr}(\boldsymbol{\kappa})$. Thus, the first term on the right measures volume-expansion caused by transport. In absence of the second term, and for constant partial molar volumes, the total flux of volume-fractions $c_{\alpha} \nu_{\alpha} \mathbf{v}_{\alpha}$ measured in the fixed frame is conserved, $\nabla \sum_{\alpha=1}^N c_{\alpha} \nu_{\alpha} \mathbf{v}_{\alpha} = 0$. The second term in eq. (61) measures volume-production by chemical reactions, and is an important source for convection in multi-component systems.

In the case of a single-component liquid, $\nabla \mathbf{v} = 0$ according to eq. (61), since by construction the only flux density relative to the center of mass motion vanishes, $\mathbf{N}_1 = 0$. This is a standard-condition for incompressibility of non-reactive media. However, it is often used for complex electrolyte-mixtures which can be a bad approximation.

From now on we consider electrolytes in the incompressible limit $\mathcal{K} \rightarrow \infty$, such that $\nu_{\alpha}^0 = \nu_{\alpha}$ becomes the general partial molar volume (defined for any state).

As we showed above, conservation of mass and charge reduce the number of independent species by two. We assign

the designated two physical species to $\alpha = 1, \alpha = 2$. The volume constraint eq. (57) allows to determine the corresponding concentrations,

$$c_1(c_3, \dots, c_N, \varrho) = \frac{1 - \nu_2 c_2 - \sum_{\alpha=3}^N \nu_\alpha c_\alpha}{\nu_1}, \quad (62)$$

$$c_2(c_3, \dots, c_N, \varrho) = \frac{z_1 - \nu_1 \varrho / F}{\nu_2 z_1 - \nu_1 z_2} + \sum_{\alpha=3}^N c_\alpha \frac{\nu_\alpha z_1 - \nu_1 z_\alpha}{\nu_1 z_2 - \nu_2 z_1},$$

with the charge density ϱ . Furthermore, we transform eq. (61) into the reduced description,

$$\nabla \mathbf{v} = -\frac{\tilde{\nu}_2}{F \tilde{z}_2} \nabla \mathcal{J} - \sum_{\alpha=3}^N \tilde{\nu}_\alpha \nabla \mathbf{N}_\alpha, \quad (63)$$

where $\tilde{\nu}_\alpha = \nu_\alpha - M_\alpha / M_1 \cdot \nu_1$ and $\tilde{\nu}_\alpha = \tilde{\nu}_\alpha - \tilde{z}_\alpha / \tilde{z}_2 \cdot \tilde{\nu}_2$ define the set of independent partial molar volumes. In particular, eq. (63) implies constant convection-profiles for electroneutral, binary electrolytes. Conversely, this also shows that pure ILs cannot sustain concentration gradients.⁶¹

3. Equations of Motion

The force law follows from momentum-balance in eq. (8) and takes the form of a generalized Navier-Stokes equation. However, we assume highly effective momentum-dissipation in such viscous media. We neglect external body forces,⁷⁹ and assume mechanical equilibrium,²¹

$$0 = \nabla \boldsymbol{\sigma} = -\mathcal{K} \nabla \sum_{\alpha=1}^N c_\alpha \nu_\alpha + \varrho \mathbf{E} + \eta \nabla^2 \mathbf{v} + (\lambda + \eta/3) \nabla (\nabla \mathbf{v}) - \sum_{\alpha=1}^N c_\alpha \nabla \frac{\partial(\rho \varphi_{\text{H}}^{\text{int}})}{\partial c_\alpha}, \quad (64)$$

Above we assumed constant viscosity-parameters, constant bulk-modulus, and isothermal conditions. Although the force law is not used in most of the battery literature,²⁰ it plays a fundamental role for highly concentrated electrolytes,⁷⁹ and ionic liquids,²¹ where Coulomb interactions compete with saturation effects.

Stress couples to transport via the volumetric term in the chemical potentials (see eq. (53)). Via this mechanism, we ensure that the complete, coupled set of mechanical and electrostatic stresses is comprised in our theory. By substitution, dissipative electric, viscous, and interaction forces contribute to the chemical potentials,

$$\nabla \mu_\alpha = -\varrho \nu_\alpha \nabla \Phi + RT \sum_{\beta} TDF_{\alpha\beta} \frac{\nabla c_\beta}{c_\beta} + \nu_\alpha \left((\lambda + \eta/3) \nabla (\nabla \mathbf{v}) + \eta \nabla^2 \mathbf{v} \right), \quad (65)$$

where $TDF_{\alpha\beta} = \sum_{\gamma,\beta} (\delta_{\alpha\gamma} - \nu_\alpha c_\gamma) (\delta_{\beta\gamma} + \partial \ln f_\gamma / \partial \ln c_\beta)$ is the thermodynamic factor. It is determined by the constitutive

equation $\sum_{\beta=1}^N (\delta_{\alpha\beta} - \nu_\alpha c_\beta) \nabla \partial(\rho \varphi_{\text{H}}^{\text{int}}) / \partial c_\beta + \nabla \ln c_\alpha / c_\alpha$, and differs from the standard form,⁸⁰ as it accounts for mean steric effects due to nonvanishing molar volumes. Note that the bulk modulus \mathcal{K} , which is not a viable material parameter in the incompressible limit, disappears in eq. (65).

Equation (65) constitutes the complete, mechanically coupled form for the chemical potentials in our electrolyte model. These thermodynamic forces obey a viscous Gibbs-Duhem relation, $\sum_{\alpha=1}^N c_\alpha (\nabla \mu_\alpha + F z_\alpha \nabla \Phi) = (\lambda + \eta) \nabla (\nabla \mathbf{v}) + \eta \nabla^2 \mathbf{v}$. In equilibrium we can write this with the thermodynamic pressure defined in eq. (51) as $\nabla p^{\text{td}} = -\varrho \nabla \Phi - \nabla (\mathbf{E} \mathbf{D}) / 2$. As consequence, strong pressure gradients emerge in electrochemical double-layers.²¹

We use Poisson's equation for the coupling of electric potential and charge density in the electrolyte, and use the dielectric constant $\epsilon_{\text{R}} = 1 + \chi$. This closes the set of complete isothermal equations,

$$\varrho = -\epsilon_{\text{R}} \epsilon_0 \Delta \Phi, \quad (66)$$

$$\frac{\partial \varrho}{\partial t} = -\nabla \mathcal{J} - \nabla (\varrho \mathbf{v}), \quad (67)$$

$$\frac{\partial c_\alpha}{\partial t} = -\nabla \mathbf{N}_\alpha - \nabla (c_\alpha \mathbf{v}), \quad \alpha \geq 3, \quad (68)$$

$$\nabla \mathbf{v} = -\frac{\tilde{\nu}_2}{F \tilde{z}_2} \nabla \mathcal{J} - \sum_{\alpha=3}^N \tilde{\nu}_\alpha \nabla \mathbf{N}_\alpha. \quad (69)$$

Equation (68) comprise N-2 independent equations for the independent concentrations c_3, \dots, c_N (where c_1 and c_2 follow from eq. (62)). Here, we restate the ionic fluxes and the conduction current density,

$$\mathbf{N}_\alpha = \frac{t_\alpha}{F \tilde{z}_\alpha} \mathcal{J} - \mathcal{D}_{\alpha T} \nabla T - \sum_{\beta=3}^N \mathcal{D}_{\alpha\beta} \nabla \tilde{\mu}_\beta, \quad \alpha \geq 3 \quad (70)$$

$$\mathcal{J} = -\kappa \nabla \varphi - \beta \kappa \nabla T - \frac{\kappa}{F} \sum_{\beta=3}^N \frac{t_\beta}{\tilde{z}_\beta} \nabla \tilde{\mu}_\beta, \quad (71)$$

which are subject to the form of the chemical potentials following from the modeled free energy density eq. (65). Note that $\varphi = \Phi + \tilde{\mu}_2 / F \tilde{z}_2$ is the reduced electrochemical potential introduced in eq. (45). Volume-expansion $\nabla \mathbf{v}$ is determined by eq. (63). Alternatively, the complete set of transport equations can be cast into matrix-form (see section SI 1 J).

In section SI 1 I, we complete the set of transport equations by deriving the equation for temperature ("heat equation"),

$$C \dot{T} = \mathcal{R} - \mu_{\text{T}} \mathcal{J} \nabla T - T \tilde{\beta} \nabla \mathcal{J} + \frac{T}{F} \nabla \tilde{D}_\varrho \nabla \varrho + T \sum_{\gamma=3}^N \tilde{D}_\gamma \nabla c_\gamma + T \nabla \tilde{\lambda} \nabla T. \quad (72)$$

III. SIMULATION OF ZINC ION BATTERY CELL

Secondary zinc-ion batteries (ZIB) are an emerging technology for safe and low-cost energy storage.⁸¹⁻⁸³ Here, we

model a secondary ZIB with IL-water mixture as electrolyte, based on the experimental work described in 41. Comparison with these experimental results serves as validation for our transport theory. First, we sketch the cell set-up and describe our modeling equations. Second, we present our simulation results.

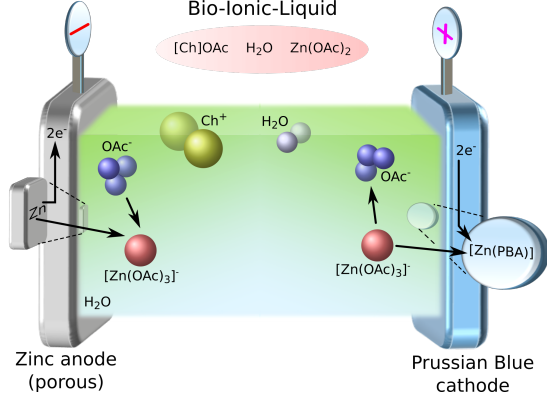


FIG. 2. Scheme of the simulated zinc-ion battery.

The electrodes consist of a porous zinc-anode (zinc powder) and a Prussian-blue-analogue (PBA) cathode ($\text{FeFe}(\text{CN})_6$). The employed electrolyte is composed of a mixture of choline acetate ($[\text{Ch}]\text{OAc}$) with 30 wt % water into which 1M of zinc acetate ($\text{Zn}(\text{OAc})_2$) is dissolved. Despite the significant amount of water, the $[\text{Ch}]\text{OAc}$ +water mixture can (still) be denoted “IL with water”.⁸⁴ See fig. 2 for an illustration of the ZIB.

A. Model Equations

We neglect hydration of the salt-ions by water and assume a complete dissociation of the salt $[\text{Ch}]\text{OAc} \rightleftharpoons \text{Ch}^+ + \text{OAc}^-$. In principle, various different ionic zinc-complexes may form under bulk-reactions, depending on the pH-value of the solution.^{85,86} However, such a detailed investigation lies beyond the scope of this paper. Thus, we assume complete complexation of the zinc-salt according to $\text{Zn}(\text{OAc})_2 + \text{OAc}^- \rightleftharpoons [\text{Zn}(\text{OAc})_3]^-$.⁸⁷ We model the electrolyte as quaternary mixture of the three charged constituents Ch^+ , OAc^- , $[\text{Zn}(\text{OAc})_3]^-$, and water.⁸⁸⁻⁹⁰ As reference, we designate water, thus $\tilde{z}_\alpha = z_\alpha$. This choice corresponds to transport theories developed for aqueous solutions, based on water as solvent.¹⁹

Since length scales above some nanometers suffice for the description of batteries,¹⁹ we can safely assume our system to be electroneutral, *viz.* $\varrho = 0$.³¹ As a consequence, the charge density is not a free variable and we solve $\partial_t \varrho = 0$ in eq. (67) for $\nabla \mathcal{J}$ instead of Poisson’s eq. (66). As thermal aspects play a minor role in elementary battery cells,²⁰ we assume thermal equilibrium at room temperature, *i.e.*, $\nabla T = 0$. Hence, the temperature appears only as constant a parameter. Here, we set the activity coefficients to $f_\alpha = 1$ and neglect non-ideal interactions $\varphi_{\text{H}}^{\text{int}} = 0$. Furthermore, we assume constant

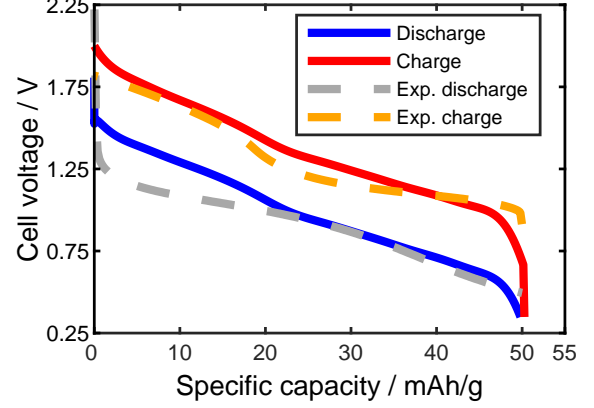


FIG. 3. Comparison of simulated and measured⁴¹ cell voltage for a galvanostatic charge-discharge cycle of the ZIB with current $j = 0.1 \text{ mA cm}^{-2}$.

viscosity-coefficients ($\eta = 25.3 \text{ mPa}$ and $\lambda = 0$)⁹¹ in the chemical potentials.

The only independent specific concentrations are c_3 and c_4 , which determine c_1 and c_2 via eq. (62), subject to the condition $\varrho = 0$.

Due to the porous cell structure, the set of transport equations must be modified by means of volume-averaging, as described by porous electrode theory.⁹² Volume-averaging over liquid and solid phases implies volumetric (ε) and dynamic (ε^β) transport-corrections, where $\varepsilon = V^l/V$ is the liquid-phase volume-fraction or porosity. β is the Bruggemann-coefficient, which depends on the microstructure,

$$\frac{\partial}{\partial t} (\varepsilon c_\alpha) |_{\alpha=3,4} = -\nabla \cdot (\varepsilon c_\alpha \mathbf{v}) - \nabla \cdot (\varepsilon^\beta \mathbf{N}_\alpha) + r_\alpha, \quad (73)$$

$$0 = \nabla \cdot (\varepsilon^\beta \mathcal{J}) = -\nabla \cdot (\varepsilon \varrho \mathbf{v}) + \sum_{\alpha=1}^4 F z_\alpha r_\alpha, \quad (74)$$

$$\nabla \cdot (\varepsilon \mathbf{v}) = \sum_{\alpha=1}^4 v_\alpha r_\alpha - \frac{\tilde{v}_2}{F \tilde{z}_2} \nabla \cdot (\varepsilon^\beta \mathcal{J}) - \sum_{\alpha=3}^4 \tilde{v}_\alpha \nabla \cdot (\varepsilon^\beta \mathbf{N}_\alpha). \quad (75)$$

Reactions occur only at the electrode surfaces and appear as source-terms in our model equations, defined as

$$r_\alpha = \sum_{k,\Gamma} a^{\Gamma} v_{k,\alpha}^{\Gamma} i^{\Gamma}. \quad (76)$$

Species	\tilde{z}_α	$c_\alpha^0 / \text{mol m}^{-3}$	Volume fraction $c_\alpha v_\alpha$
$\alpha=1$: H_2O (designated)	0	$19.43 \cdot 10^3$	0.35
$\alpha=2$: Ch^+	1	$5.00 \cdot 10^3$	0.35
$\alpha=3$: OAc^-	-1	$4.00 \cdot 10^3$	0.22
$\alpha=4$: $[\text{Zn}(\text{OAc})_3]^-$	-1	$1.00 \cdot 10^3$	0.08

TABLE I. Species assignment and initial electrolyte composition. Since water is the designated species, $\tilde{z}_\alpha = z_\alpha$. Note the minor volume fraction of the critical $[\text{Zn}(\text{OAc})_3]^-$ -salt.

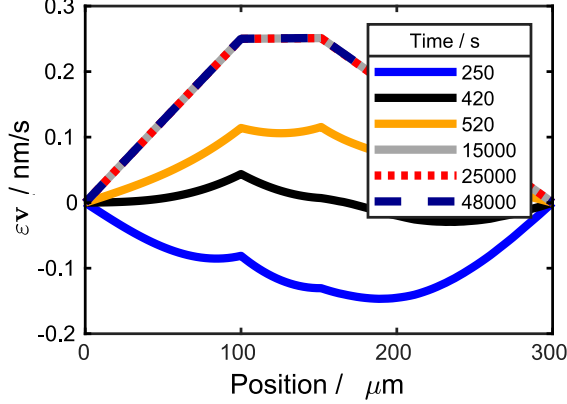
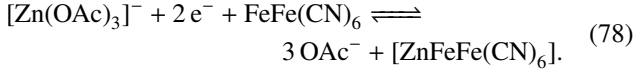
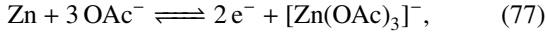


FIG. 4. Volume-averaged convection velocities at the designated moments (see fig. SI 1) during discharge of the ZIB with current $j = 0.1 \text{ mA cm}^{-2}$.

This sum includes all reactions k at all electrode-interfaces Γ , involving species α . Here, $\nu_{k;\alpha}^F$ are the stoichiometries of the reactions, and the specific surfaces a^F measure the surface-to-volume ratio of the electrode Γ . The specific surface-reaction-rate i^F constitutes interface-conditions between the solid and liquid phase, and depends upon the reaction overpotential. We model this quantity using a Butler-Vollmer-Ansatz,⁹³ see section SI 1 L.

The half cell reactions occurring at the Zn-anode and the PBA-cathode ($\text{FeFe}(\text{CN})_6$) are (see section SI 2 A)



Thus, zinc dissolves from the anode and intercalates into the cathode (and vice versa). We neglect solid-state diffusion and model the cathodic reactions as deposition-processes (see section SI 2 B 1).

B. Simulation Results

In this section, we present the simulation results of the as-modeled ZIB and compare them with the experimental results (we specify our numerical methods in section SI 2 C).⁴¹ In this way, we study the spatial profile and temporal evolution of concentrations and convection velocity. We highlight the relevance of convection for cell performance and compare possible definitions of transference numbers.

1. Competition of Diffusion, Migration, and Convection

First, we validate our model. For this purpose, we simulate the galvanostatic discharge and charge of the ZIB by applying

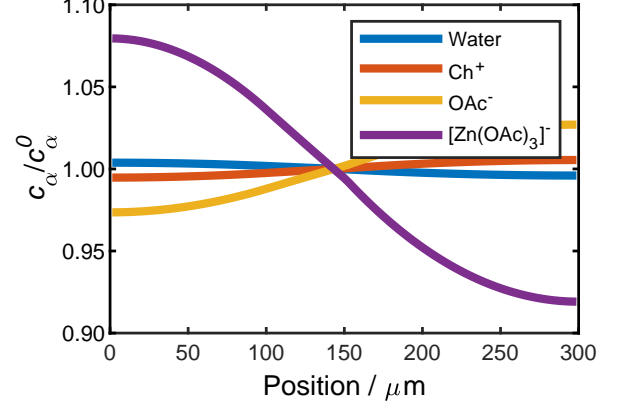


FIG. 5. Typical concentration profiles for the quaternary electrolyte-composition at the end of discharge with current $j = 0.1 \text{ mA cm}^{-2}$. The initial electrolyte composition, c_α^0 , is tabulated in table I

a moderate current density ($j = 0.1 \text{ mA cm}^{-2}$). We compare our simulation results with experimental observations in fig. 3. Apparently, the specific capacities and cell voltages obtained from simulation are in good agreement with the experimental values. However, the discharge profile obtained from experiment exhibits two discharge phases with a transition at approximately 20 mA h g^{-1} . Endres et al.⁴¹ attribute this effect to two different electro-reactivities, stemming from low-/ and high-spin states of Fe(III) in the PBA. Because such atomistic processes lie beyond the scope of our model in this paper, this transition is not found in simulations.

Our model provides a complete description of the electrolyte dynamics. In the following, we discuss the ion dynamics and their influence on the overall cell performance in order to understand the interplay between the different transport mechanisms (migration, diffusion, and convection), and the reactions at the electrode surfaces.

For a proper discussion of the electrolyte evolution during discharge of the battery, we designate some characteristic moments. Figure SI 1 shows the discharge-profile of the cell-voltage and the designated moments. We set one focus on processes occurring during the initial discharge-phase ($t = 250 \text{ s}, 420 \text{ s}, 520 \text{ s}$). Furthermore, we designate two intermediate moments, and, finally, the moment of complete discharge of the cell. The significance of the designated times becomes apparent below when evaluating the electrolyte-quantities Φ , \mathbf{v} , and c_α at these moments.

Figure 4 shows the temporal evolution of the convection velocity profile. Apparently, the direction of the motion of the center-of-mass switches from towards the anode (negative convection), to towards the cathode (positive convection) right after the initial phase, and, then, the profile quickly becomes quasi-stationarity. In the supplementary, we observe a similar behavior for the ionic concentrations (see fig. SI 1c-f). Initially (first three designated moments), concentration-differentials grow throughout the cell, followed by quasi-stationary profiles during the rest of the discharge.

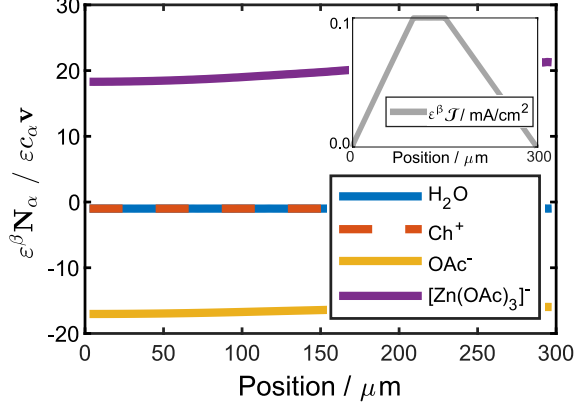


FIG. 6. Convection contribution to ionic mass fluxes at the end of discharge. The inset shows the conduction current density $\varepsilon^\beta \mathcal{J}$ at end of discharge with current $j = 0.1 \text{ mA cm}^{-2}$.

We explain these observations with the push of the electrolyte out of its initial equilibrium-state by the application of the external current. As the system relaxes towards the new stationary state under galvanostatic discharge, the concentrations approach stationary profiles. Before concentration gradients are built up, convection transports zinc from anode to cathode. As zinc is dissolved as complex $[\text{Zn}(\text{OAc})_3]^-$, a net loss of available electrolyte volume occurs at the cathode, and a net gain of electrolyte volume at the anode. This pushes electrolyte from cathode to anode according to eq. (75) and results in negative convection velocities. We give a detailed analysis of the electrolyte-dynamics in the SI (see section SI 3 A).

The evolution of the electric potential in the electrolyte is shown in Figure SI 1 b). As expected, the cathode is more electronegative than the anode ($\Delta\Phi^{\text{cell}} \approx -0.1 \text{ mV}$) at all times during discharge. This implies a migrational pull of the anionic species towards the cathode, and of the Ch^+ -ions towards the anode. Thus, migration hinders cell operation, which depends on negative $[\text{Zn}(\text{OAc})_3]^-$ -ions. As a consequence, diffusion and convection must overcompensate the electric forces in the electrolyte to sustain cell operation.

Figure 5 shows normalized, quasi-stationary concentration-profiles of all electrolyte species at end-of-discharge. Interestingly, the gradients of the two anionic species (OAc^- and $[\text{Zn}(\text{OAc})_3]^-$) have opposite orientations. The profile for the positively charged Ch^+ -ions moderately increases at the more electronegative cathode. Likewise, water shows a small gradient, despite being neutral ($\tilde{z}_{\text{H}_2\text{O}} = 0$ in this reference-frame) and thus not being susceptible to migration.

Most importantly, the large concentration gradient of the $[\text{Zn}(\text{OAc})_3]^-$ -ions is necessary to overcome the migration pull. This is mandatory to maintain cell operation, as zinc is intercalated into the cathodic PBA-structure. OAc^- -ions have to move back to the anode, which is realized by a small concentration gradient and the migration pull. This motion of bulky OAc^- -ions induces the positive convection velocity

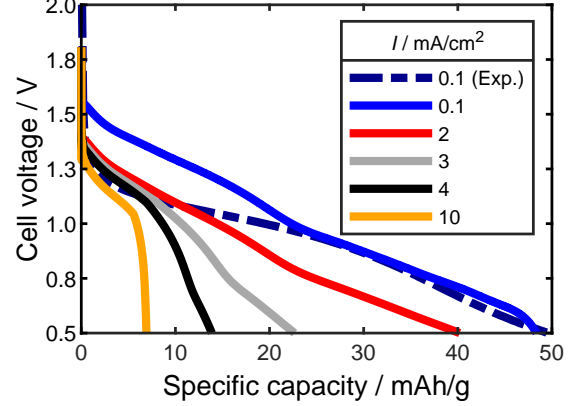


FIG. 7. Cell voltage during discharge for various current densities.

during the stationary phase of galvanostatic discharge seen in fig. 4 (see eq. (75)).

Figure 6 illustrates the relevance of convective transport for the electrolyte-species. The ratio $\varepsilon^\beta \mathbf{N}_\alpha / \varepsilon c_\alpha \mathbf{v}$ shows the relation between flux densities within the center-of-mass system and the center-of-mass velocities. This ratio is larger than one (roughly one), if convection is negligible (dominant) in transport of the respective species. Apparently, convective flux contributions are negligible for the two negative species, whereas convection plays a significant role for the dynamics of water and Ch^+ -ions. Thus, convection is important for those species that do not contribute to the half-cell reactions. We infer from the sign of the ratio $\varepsilon^\beta \mathbf{N}_\alpha / \varepsilon c_\alpha \mathbf{v}$ that OAc^- -ions move towards the anode, whereas $[\text{Zn}(\text{OAc})_3]^-$ -ions moves towards the cathode. This confirms our previous finding for the $[\text{Zn}(\text{OAc})_3]^-$ -ions that diffusion overcompensates migration.

2. Limiting Discharge Currents

Now, we investigate the power limiting mechanisms of this ZIB with IL electrolyte. For this purpose, we simulate the cell discharge at high current densities.

Figure 7 illustrates the impact of increased discharge currents on the overall cell performance. The shape of the discharge profile is preserved for moderate discharge current densities (up to $I = 2 \text{ mA cm}^{-2}$), despite being shifted to smaller discharged capacities. At higher current densities, a strong capacity fade is observed and the discharge profiles exhibit steep voltage drops.

These voltage drops suggest that diffusion becomes too slow to supply the cathodic interfacial reaction mechanism with sufficient amount of $[\text{Zn}(\text{OAc})_3]^-$ -salt. Such a behavior is typical for ILs, which are often highly viscous.⁹⁴

This explanation is confirmed by fig. 8, in which the concentration profiles of the $[\text{Zn}(\text{OAc})_3]^-$ -ions for the different discharge currents at the end of discharge is shown. We ob-

serve steep concentration gradients throughout the cell. The salt concentration at the cathode decreases with increasing discharge currents, and, finally, $[\text{Zn}(\text{OAc})_3]^-$ -ions get depleted.

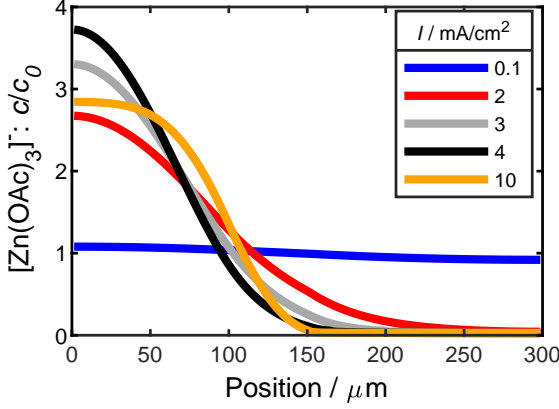


FIG. 8. Concentration profiles of $[\text{Zn}(\text{OAc})_3]^-$ at end of discharge state for various discharge current densities.

At intermediate current densities, we observe in fig. 8 that the $[\text{Zn}(\text{OAc})_3]^-$ concentration at the anode increases with discharge current density. Interestingly, it starts to decrease for very high current densities. In this case, the cell fails so quickly due to diffusion limitation that a quasi-stationary concentration-profile cannot establish.

3. Discussion of Transference Numbers

Finally, we demonstrate the consistency of our transport theory. In our model, we choose two reference species because of momentum and charge conservation. The model predictions should be independent of this choice. Here, we compare simulations with different reference species.

In the theory-chapter, we showed that all $N(N+1)/2$ transport-parameters, appearing in a N -component electrolyte-mixture, follow from the Onsager matrix \mathcal{L} , see eqs. (36) to (40). Although the designated species does not appear explicitly, \mathcal{L} comprises the complete set of inter-species-correlations, including correlations involving the designated species. This becomes apparent in the closure-relation for the independent fluxes $\mathbf{N}_\alpha|_{\alpha \geq 2}$, eq. (31), which implicitly determines \mathbf{N}_1 . Thus, the Onsager-matrices with respect to different designated species are mutually coupled, and cannot be stated independently from each other. In section SI 1 K we show that simple conversion relations exist, which allow to transfer between the different choices of reference species.

In section SI 3 B we prove consistency of our framework. Figure SI 3 shows a comparison of the discharge curves and the final concentration profiles of the $[\text{Zn}(\text{OAc})_3]^-$ -ions, obtained by simulations using the three different sets of reference species comprised in table II. Apparently, the deviations

lie within numerical accuracy (relative error $\approx O(10^{-6})$). This is consistent, since both cell voltage and concentrations must not depend upon the choice of reference. Thus, they give, up to numerical accuracy, identical results.

In contrast to the electric conductivity, some transport parameters, e.g., transference numbers, depend on the choice of reference species. Figure 9 shows the transference numbers at the end of discharge for two different reference species. In addition, table II summarizes spatially averaged values of the transference numbers at end of discharge, for three different sets of reference species. In quaternary electrolytes, only two transference numbers are independent and only three transference numbers are well-defined.

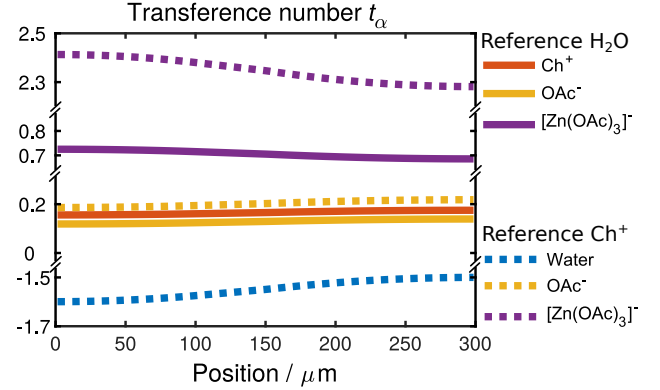


FIG. 9. Transference numbers at end of discharge for the reference species H_2O , and Ch^+ .

We observe in fig. 9 that sign and magnitude of the transference numbers depends on the reference species chosen due to momentum conservation. Interestingly, t_{OAc^-} is rather similar for both reference species H_2O , and Ch^+ , respectively. A significant discrepancy is observed for $t_{[\text{Zn}(\text{OAc})_3]^-}$. When Ch^+ as charged species is designated, water acquires an effective

Reference	Species	\tilde{z}_α	t_α
Water	Water	0	<i>n.d.</i>
	Ch^+	1	0.166
	OAc^-	-1	0.129
	$[\text{Zn}(\text{OAc})_3]^-$	-1	0.705
Ch^+	Water	-0.170	-1.549
	Ch^+	0	<i>n.d.</i>
	OAc^-	-1.570	0.203
	$[\text{Zn}(\text{OAc})_3]^-$	-3.330	2.346
$[\text{Zn}(\text{OAc})_3]^-$	Water	0.074	0.665
	Ch^+	1.430	0.237
	OAc^-	-0.757	0.098
	$[\text{Zn}(\text{OAc})_3]^-$	0	<i>n.d.</i>

TABLE II. Results for the transference-numbers obtained from using different reference-frames. The numbers were obtained from spatially-averaging over the cell. No transference-numbers for the designated species ($\alpha = 1$) exist relative to the center-of-mass motion (*n.d.*, not defined). In particular, $\sum_{\alpha=2}^N t_\alpha = 1$ in each frame.

charge, and thus contributes to the electric current. In particular, $t_{\text{H}_2\text{O}}$ is negative in the Ch^+ -frame.

Transference numbers are particularly intuitive for the neutral reference species H_2O . In this setting, the signs of transference numbers endorse our interpretation of the overall electrolyte dynamics, discussed above.

Table II and the inset in fig. 6 imply that at end of discharge $t_{[\text{Zn}(\text{OAc})_3]^-} \mathcal{J}/z_{[\text{Zn}(\text{OAc})_3]^-} < 0$, whereas figs. 4 and 6 imply $\mathbf{N}_{[\text{Zn}(\text{OAc})_3]^-} > 0$. Thus, diffusion dominates over migration and is the main driving force for cell operation (see eq. (43)).

The relations between the numerical results for the transference numbers obtained in the three different reference-frames agree with the analytical predictions, see eqs. (SI 122a) to (SI 122f).

Since, there is an ongoing debate regarding the sign and magnitude of transference numbers in concentrated electrolytes and ionic liquids,^{63,64} we shall briefly comment on this topic here.

Various, differing definitions for transport parameters exist in the literature, which bears the potential for confusion when comparing results from different authors. Thus, a complete characterization should state all transference numbers and make their definitions clear. In our theory, we define transference numbers and diffusion coefficients relative to the bulk-motion of the center-of-mass. As it was shown earlier for molten salts,⁶² such an internal description predicts that transference numbers can take up any real value if the Onsager matrix contains off-diagonal terms. Some works in the literature perform a less general approach and choose one specific ionic species as internal reference,⁹⁵ or choose an external description using fixed coordinates as reference.⁹⁶ Since each approach bears its own experimental significance,⁹⁷ we resolve this ambiguity in section SI I G. There, we derive simple relations, which transform between the different reference-systems.

Of course, the theoretical concepts must be probed by experiments. However, the experimental determination of transport parameters in concentrated electrolytes is challenging. In principle, suitable methods must take into account all inter-species-correlations and the formation of ionic clusters and ion-aggregates.⁹⁸ In particular, applicability of NMR/PFG-NMR experiments for determination of transport parameters is limited for concentrated electrolytes, as they (i) neglect formation of ionic complexes, (ii) derive transference numbers from diffusion coefficients via Nernst-Einstein relations strictly valid only for ideal electrolytes and (iii) provide only averaged values.⁶⁴ Recently, the measurement of ionic electrophoretic mobilities was proposed to overcome these obstacles, either using non-blocking electrodes,⁶⁷ or experiments based on electrophoretic NMR (eNMR).^{99,100} Unfortunately, the first technique does not apply to neat IL, as it is not suitable for non-metal ions.¹⁰¹ In contrast, eNMR applies to both, neat ILs and Li-IL-mixtures.⁶³ In principle, this method is evaluated with the external fixed laboratory-frame as reference. However, this is correct only if convection is negligible (see

eq. (SI 27)).

IV. CONCLUSIONS

To the best of our knowledge, we have developed the first thermodynamically consistent transport theory applicable for pure ILs. Our theory describes the complete set of coupled transport equations for composition (concentration), temperature, charge density, electric potential, and convection. We make explicit use of the force law to include all mechanical couplings. Our detailed equations for the electrolyte dynamics describe the individual contributions of all species to transport of mass, charge, heat, and to convection.

The present work completes our two-fold validation procedure. In a first publication, the theory was validated in a joint experimental/theoretical investigation of the double-layer-structures formed by a binary IL near an electrified interface, and of how a ternary salt influences these characteristic IL-structures.²¹ Here, we apply the electroneutral transport theory to a complete secondary battery cell.

Our simulations determine the concentration dependent electrolyte dynamics during a complete cycle of discharging-charging of a secondary zinc-ion battery based on an IL-electrolyte. The resulting discharge profile is in good agreement with the experimental results. However, the cell performance is limited by the negativity of the zinc ions. These must overcome a Coulombic potential barrier to maintain cell operation by the formation of concentration gradients. In contrast to binary ILs, convection does not play a significant role compared to the competing mechanisms of migration and diffusion.

Our theory provides a rigorous framework for the determination of the transport parameters, which all follow from the fundamental Onsager matrix. Furthermore, we enrich the present discussion regarding the interpretation of transport parameters in solvent-free electrolytes, as they depend on different reference-frames. Our model clarifies the exact number of independent parameters and contains simple equations for their conversions.

The generality of the presented framework covers a huge variety of physico-chemical systems and it can be customized by appropriate free energy models. In particular, it applies to electroneutral cell-systems as well as to confined geometries near electrified interfaces. Our transport theory thus provides a valid framework for the description of complex, multi-component battery-electrolytes in general (concentrated electrolytes, water-in-salt-electrolytes, ILs) as well as for the description of surface-effects of ILs and IL-mixtures.

V. ACKNOWLEDGEMENT: LUZI/BMBF

This work was supported by the German Ministry of Education and Research (BMBF) (project LUZI, BMBF: 03SF0499E).

- [1] G. Crabtree, E. Kócs, and L. Trahey, *MRS Bulletin* **40**, 1067 (2015).
- [2] M. Armand and J.-M. Tarascon, *Nature* **451**, 652 (2008).
- [3] S. Clark, A. R. Mainar, E. Iruin, L. C. Colmenares, J. A. Blázquez, J. R. Tolchard, Z. Jusys, and B. Horstmann, *Advanced Energy Materials* **10**, 1903470 (2020).
- [4] S. Hein, T. Danner, D. Westhoff, B. Prifling, R. Scurtu, L. Kremer, A. Hoffmann, A. Hilger, M. Osenberg, I. Manke, *et al.*, *Journal of The Electrochemical Society* **167**, 013546 (2020).
- [5] S. Braun, C. Yada, and A. Latz, *The Journal of Physical Chemistry C* **119**, 22281 (2015).
- [6] D. R. MacFarlane, N. Tachikawa, M. Forsyth, J. M. Pringle, P. C. Howlett, G. D. Elliott, J. H. Davis, M. Watanabe, P. Simon, and C. A. Angell, *Energy Environ. Sci.* **7**, 232 (2014).
- [7] M. Armand, F. Endres, D. R. MacFarlane, H. Ohno, and B. Scrosati, *Nature Materials* **8**, 621 (2009).
- [8] N. V. Plechkova and K. R. Seddon, *Chem Soc Rev* **37**, 123 (2008).
- [9] M. Galiński, A. Lewandowski, and I. Stępnia, *Electrochimica Acta* **51**, 5567 (2006).
- [10] M. Freemantle, *An Introduction to Ionic Liquids* (The Royal Society of Chemistry, 2009).
- [11] Z. Liu, G. Pulletikurthi, A. Lahiri, T. Cui, and F. Endres, *Dalton Trans.* **45**, 8089 (2016).
- [12] S. Mallakpour and Z. Rafiee, *Journal of Polymers and the Environment* **19**, 447 (2011).
- [13] R. Hayes, G. G. Warr, and R. Atkin, *Chemical Reviews* **115**, 6357 (2015).
- [14] M. V. Fedorov and A. A. Kornyshev, *Chemical Reviews* **114**, 2978 (2014).
- [15] N. Gavish and A. Yochelis, *The Journal of Physical Chemistry Letters* **7**, 1121 (2016).
- [16] N. Gavish, D. Elad, and A. Yochelis, *The Journal of Physical Chemistry Letters* **9**, 36 (2018).
- [17] A. Yochelis, M. B. Singh, and I. Visoly-Fisher, *Chemistry of Materials* **27**, 4169 (2015).
- [18] S. Bier, N. Gavish, H. Uecker, and A. Yochelis, *Phys. Rev. E* **95**, 060201 (2017).
- [19] A. Latz and J. Zausch, *Journal of Power Sources* **196**, 3296 (2011).
- [20] A. Latz and J. Zausch, *Beilstein Journal of Nanotechnology* **6**, 987 (2015).
- [21] V. Hoffmann, G. Pulletikurthi, T. Carstens, A. Lahiri, A. Borodin, M. Schammer, B. Horstmann, A. Latz, and F. Endres, *Phys. Chem. Chem. Phys.* **20**, 4760 (2018).
- [22] J. Wu, T. Jiang, D.-e. Jiang, Z. Jin, and D. Henderson, *Soft Matter* **7**, 11222 (2011).
- [23] O. Hollóczki, F. Malberg, T. Welton, and B. Kirchner, *Phys. Chem. Chem. Phys.* **16**, 16880 (2014).
- [24] J. Jiang, D. Cao, D.-e. Jiang, and J. Wu, *Journal of Physics: Condensed Matter* **26**, 284102 (2014).
- [25] C. J. Margulis, *Molecular Physics* **102**, 829 (2004).
- [26] J. N. Canongia Lopes, M. F. Costa Gomes, and A. A. Pádua, *The Journal of Physical Chemistry B* **110**, 16816 (2006).
- [27] S. Yeganegi, A. Soltanabadi, and D. Farmanzadeh, *The Journal of Physical Chemistry B* **116**, 11517 (2012).
- [28] S. Li, G. Feng, J. L. Bañuelos, G. Rother, P. F. Fulvio, S. Dai, and P. T. Cummings, *The Journal of Physical Chemistry C* **117**, 18251 (2013).
- [29] S. Sharma, A. Gupta, and H. K. Kashyap, *The Journal of Physical Chemistry B* **120**, 3206 (2016).
- [30] M. Z. Bazant, B. D. Storey, and A. A. Kornyshev, *Phys. Rev. Lett.* **106**, 046102 (2011).
- [31] J. Newman and K. Thomas-Alyea, *Electrochemical Systems*, The ECS Series of Texts and Monographs (Wiley, 2012).
- [32] W. Dreyer, C. Gohlke, and R. Müller, *Entropy* **20**, 939 (2018).
- [33] C. Gohlke, Ph.D. thesis, TU-Berlin, Berlin, Germany (2015).
- [34] R. Hayes, N. Borisenko, M. K. Tam, P. C. Howlett, F. Endres, and R. Atkin, *The Journal of Physical Chemistry C* **115**, 6855 (2011).
- [35] F. Single, B. Horstmann, and A. Latz, *The Journal of Physical Chemistry C* **123**, 27327 (2019).
- [36] T. Cui, A. Lahiri, T. Carstens, N. Borisenko, G. Pulletikurthi, C. Kuhl, and F. Endres, *The Journal of Physical Chemistry C* **120**, 9341 (2016).
- [37] J.-P. Hansen and I. R. McDonald, eds., *Theory of Simple Liquids (Fourth Edition)*, fourth edition ed. (Academic Press, Oxford, 2013).
- [38] L. Suo, O. Borodin, T. Gao, M. Olguin, J. Ho, X. Fan, C. Luo, C. Wang, and K. Xu, *Science* **350**, 938 (2015).
- [39] Z. Liu, G. Pulletikurthi, and F. Endres, *ACS Applied Materials & Interfaces* **8**, 12158 (2016).
- [40] K. R. Seddon, A. Stark, and M.-J. Torres, *Pure and Applied Chemistry* **72**, 2275 (01 Jan. 2000).
- [41] Z. Liu, P. Bertram, and F. Endres, *Journal of Solid State Electrochemistry* **21**, 2021 (2017).
- [42] S. Kovetz and A. Kovetz, *Electromagnetic Theory*, Oxford science publications (Oxford University Press, 2000).
- [43] S. de Groot and P. Mazur, *Non-equilibrium Thermodynamics*, Dover Books on Physics (Dover Publications, 1984).
- [44] G. Lebon, D. Jou, and J. Casas-Vázquez, *Understanding non-equilibrium thermodynamics*, Vol. 295 (Springer, 2008).
- [45] I. Müller, *Archive for Rational Mechanics and Analysis* **45**, 241 (1972).
- [46] I. Müller, *A history of thermodynamics: the doctrine of energy and entropy* (Springer Science & Business Media, 2007).
- [47] I. Liu, *Continuum Mechanics*, Advanced Texts in Physics (Springer Berlin Heidelberg, 2002).
- [48] L. G. Leal, *Advanced transport phenomena: fluid mechanics and convective transport processes*, Vol. 7 (Cambridge University Press, 2007).
- [49] K. Henjes, *Annals of Physics* **223**, 277 (1993).
- [50] R. Medina and J. Stephany, The force density and the kinetic energy-momentum tensor of electromagnetic fields in matter (2014), [arXiv:1404.5250](https://arxiv.org/abs/1404.5250).
- [51] I. Müller, *Thermodynamics*, Interaction of Mechanics and Mathematics Series (Pitman, 1985).
- [52] F. A. Reich, W. Rickert, and W. H. Müller, *Continuum Mechanics and Thermodynamics* **30**, 233 (2018).
- [53] P. Kinsler, A. Favaro, and M. W. McCall, *European Journal of Physics* **30**, 983 (2009).
- [54] E. Poisson, *A Relativist's Toolkit: The Mathematics of Black-Hole Mechanics* (Cambridge University Press, 2004).
- [55] C. Truesdell, *Rational thermodynamics* (Springer Science & Business Media, 2012).
- [56] J. D. Jackson, *Classical electrodynamics* (John Wiley & Sons, 2007).
- [57] K. Hutter, A. A. Ven, and A. Ursescu, *Electromagnetic Field Matter Interactions in Thermoelastic Solids and Viscous Fluids*, Vol. 710 (Springer, 2007).
- [58] W. Noll, *Archiv der Mathematik* **21**, 87 (1970).
- [59] C. De Boor, *Journal of Elasticity* **15**, 225 (1985).

- [60] L. Martins, *Journal of elasticity* **54**, 89 (1999).
- [61] G. Mamantov and R. Marassi, *Molten salt chemistry: an introduction and selected applications*, Vol. 202 (Springer Science & Business Media, 2012).
- [62] S. K. Ratkje, H. Rajabu, and T. Førland, *Electrochimica Acta* **38**, 415 (1993).
- [63] M. Gouverneur, F. Schmidt, and M. Schönhoff, *Phys. Chem. Chem. Phys.* **20**, 7470 (2018).
- [64] K. R. Harris, *Phys. Chem. Chem. Phys.* **20**, 30041 (2018).
- [65] D. Bothe and W. Dreyer, *Acta Mechanica* **226**, 1757 (2015).
- [66] P. Goyal and C. W. Monroe, *Journal of The Electrochemical Society* **164**, E3647 (2017).
- [67] F. Wohde, M. Balabajew, and B. Roling, *Journal of The Electrochemical Society* **163**, A714 (2016).
- [68] G. Hütter, *Continuum Mechanics and Thermodynamics* **28**, 1935 (2016).
- [69] B. D. Coleman and W. Noll, *Archive for Rational Mechanics and Analysis* **13**, 167 (1963).
- [70] G. K. Batchelor, *An Introduction to Fluid Dynamics*, Cambridge Mathematical Library (Cambridge University Press, 2000).
- [71] K. Binnemans, *Chemical Reviews* **105**, 4148 (2005).
- [72] R. Becker and F. Sauter, *Theorie der Elektrizität* (Springer, 1933).
- [73] V. Freise, *Zeitschrift für Elektrochemie* **56**, 822 (1952).
- [74] B. Horstmann, T. Danner, and W. G. Bessler, *Energy & Environmental Science* **6**, 1299 (2013).
- [75] W. Dreyer, C. Guhlke, and R. Müller, *Phys. Chem. Chem. Phys.* **17**, 27176 (2015).
- [76] F. Single, B. Horstmann, and A. Latz, *Journal of The Electrochemical Society* **164**, E3132 (2017).
- [77] J. Stamm, A. Varzi, A. Latz, and B. Horstmann, *Journal of Power Sources* **360**, 136 (2017).
- [78] T. Schmitt, T. Arlt, I. Manke, A. Latz, and B. Horstmann, *Journal of Power Sources* **432**, 119 (2019).
- [79] W. Dreyer, C. Guhlke, and R. Müller, *Phys. Chem. Chem. Phys.* **15**, 7075 (2013).
- [80] J. Landesfeind, A. Ehrl, M. Graf, W. A. Wall, and H. A. Gasteiger, *Journal of The Electrochemical Society* **163**, A1254 (2016).
- [81] S. Clark, N. Borchers, Z. Jusys, R. J. Behm, and B. Horstmann, Aqueous zinc batteries, in *Encyclopedia of Electrochemistry* (Wiley Online Library, 2020) pp. 1–54.
- [82] C. Xu, B. Li, H. Du, and F. Kang, *Angewandte Chemie International Edition* **51**, 933 (2012).
- [83] S. Liu, W. Han, B. Cui, X. Liu, F. Zhao, J. Stuart, and S. Licht, *Journal of Power Sources* **342**, 435 (2017).
- [84] Z. Liu, S. Z. El Abedin, and F. Endres, *ChemPhysChem* **16**, 970 (2015).
- [85] S. Clark, A. Latz, and B. Horstmann, *ChemSusChem* **10**, 4735 (2017).
- [86] S. Clark, A. R. Mainar, E. Iruin, L. C. Colmenares, J. A. Blázquez, J. R. Tolchard, A. Latz, and B. Horstmann, *J. Mater. Chem. A* **7**, 11387 (2019).
- [87] P. D. Vreese, A. Skoczylas, E. Mattheijs, J. Franssaer, and K. Binnemans, *Electrochimica Acta* **108**, 788 (2013).
- [88] M. L. Williams, *CRC Handbook of Chemistry and Physics, 76th edition*, Vol. 53 (BMJ Publishing Group, 1996) pp. 504–504.
- [89] J. A. Riddick, W. B. Bunger, and T. K. Sakano, *Organic solvents: physical properties and methods of purification* (John Wiley and Sons, New York, NY, 1986).
- [90] R. Fleming, *Journal of the Chemical Society (Resumed)*, 4914 (1960).
- [91] IoLiTec Ionic Liquids Technologies GmbH, Private Communication (2017).
- [92] T. Schmitt, A. Latz, and B. Horstmann, *Electrochimica Acta* **333**, 135491 (2020).
- [93] A. Latz and J. Zausch, *Electrochimica Acta* **110**, 358 (2013).
- [94] N. Wongtharom, T.-C. Lee, C.-H. Wang, Y.-C. Wang, and J.-K. Chang, *J. Mater. Chem. A* **2**, 5655 (2014).
- [95] C. Sinistri, *The Journal of Physical Chemistry* **66**, 1600 (1962).
- [96] R. Haase, *Zeitschrift für Naturforschung A* **28**, 1897 (1973).
- [97] B. R. Sundheim, *The Journal of Physical Chemistry* **60**, 1381 (1956).
- [98] N. M. Vargas-Barbosa and B. Roling, *ChemElectroChem* **7**, 367 (2020).
- [99] M. Bielejewski, M. Giesecke, and I. an Furó, *Journal of Magnetic Resonance* **243**, 17 (2014).
- [100] M. Holz, *Chem. Soc. Rev.* **23**, 165 (1994).
- [101] M. Gouverneur, J. Kopp, L. van Wüllen, and M. Schönhoff, *Phys. Chem. Chem. Phys.* **17**, 30680 (2015).